Engineering Structures 108 (2016) 28–46

Contents lists available at ScienceDirect

Engineering Structures

journal homepage: www.elsevier.com/locate/engstruct

Thunderstorm response spectrum technique: Theory and applications

Giovanni Solari *

Department of Civil, Chemical and Environmental Engineering (DICCA), Polytechnic School, University of Genoa, Via Montallegro, 1, 16145 Genoa, Italy

ARTICLE INFO

Article history:
Received 7 April 2015
Revised 26 August 2015
Accepted 17 November 2015

Keywords:
Dynamic response
Equivalent wind spectrum technique
Response spectrum
Seismic engineering
Multi-Degree-Of-Freedom system
Synoptic wind
Thunderstorm
Wind Engineering

ABSTRACT

This paper is part of a research project that started from the consideration that thunderstorms are transient phenomena with short duration and the structural response to transient phenomena, most notably to earthquakes, is traditionally evaluated by the response spectrum technique. Based on this consideration, a "new" method is formulated that generalizes the "old" response spectrum technique from earthquakes to thunderstorms. A previous paper addressed this problem for ideal point-like Single-Degree-Of-Freedom systems subjected to wind actions perfectly coherent over the exposed structural surface. The present paper generalizes this formulation to real space Multi-Degree-Of-Freedom systems subjected to partially coherent wind fields with assigned velocity profile and turbulence properties; for sake of simplicity, in this stage of the research, the structure is modeled as a continuous slender vertical cantilever beam. Analyses are carried out by making recourse to the equivalent wind spectrum technique, a method developed for synoptic stationary winds, the use of which is extended here to non-synoptic non-stationary conditions. In spite of a rather complex formulation, the application of the thunderstorm response spectrum technique is straightforward: the equivalent static force is the product of the peak wind loading by a non-dimensional quantity, the equivalent response spectrum, given by a simple diagram. Its derivation represents one of the most typical features of this method: it is based on the joint numerical processing of a set of measured thunderstorm records and an analytical model that conceptually reconstructs the complete wind field around the measured data. In virtue of its characteristics, the thunderstorm response spectrum technique is particularly suitable for rapid engineering calculations and simple code applications.

1. Introduction

Extra-tropical cyclones are synoptic-scale atmospheric phenomena that strike the areas in mid-latitudes, developing on a few thousand kilometers on the horizontal, with frequency and duration of a few days. Their genesis, life-cycle and properties have been explained by the polar front theory formulated by Bjerknes and Solberg in 1922 [1].

The study of the wind actions and effects on structures due to extra-tropical cyclones is traditionally inspired by the principles introduced by Davenport in 1961 [2]. In such a framework the mean wind velocity, usually considered as horizontal, is characterized by a vertical profile in equilibrium with an atmospheric boundary layer whose depth is in the order of 1–3 km; here, within time intervals between 10 min and 1 h, the turbulent fluctuations are dealt with as stationary and Gaussian. The wind velocity is transformed into an aerodynamic loading by assuming that the turbulence is small and neglecting the quadratic term of the fluctuations; so, like the wind velocity, also the aerodynamic loading is Gaussian. Thus, dealing with structures with elastic linear behavior, also their response is Gaussian. In addition, the maximum response is modeled through a distribution function obtained assuming that the up-crossings of a suitably high response threshold are rare and independent events [3]. In this way, the probability density function of the maximum response is narrow and sharp, and its mean value may be considered as representative of the maximum response. This favored the formulation of the gust response factor technique [2,4], and the derivation of closed form solutions for rapid engineering calculations [5–7] and code applications [8]. In spite of a huge literature aiming to generalize and improve this method in several ways [9–13], the analysis of the wind-excited response of structures subjected to extra-tropical is still mainly based on the original Davenport's method [2].

Thunderstorms are meso-scale atmospheric phenomena that strike most areas of Earth, developing in a few kilometers on the horizontal. As explained by Byers and Braham in 1949 [14], they consist of a set of cells that evolves through three subsequent stages in about 30 min: in the cumulus stage a convective updraft of warm air gives rise to a large size cumulus; in the mature stage

* Tel.: +39 010 353 2940.
E-mail address: giovanni.solari@unige.it

http://dx.doi.org/10.1016/j.engstruct.2015.11.012
0141-0296/

the cumulus becomes a cumulonimbus and a downdraft of cold air occurs; in the dissipating stage the thunderstorm is first dominated by the downdraft, then it disappears. In the '70s and in the '80s Fujita showed that the downdraft that impinges over the ground produces intense radial outflows; he called downburst the whole of these air movements [15]. On the one hand, these findings gave rise to a fervour of research in atmospheric sciences, which focused on the causes, morphology and life-cycle of thunderstorms [16]. On the other hand, they revealed that design wind actions and effects on structures are often due to thunderstorms, so they have a focal role on the structural safety; this caused a striking research in wind engineering [17,18], where two main lines have been followed.

The first line is based on the simulation of the thunderstorm wind field by wind tunnel tests [17,19–22], CFD codes [20,23–26] and advanced analytical models [27–30]. The use of wind tunnel tests allows to derive the structural loading and possibly the dynamic response in the course of the experiments. The use of CFD codes and analytical models calls for the transformation of the wind field into aerodynamic wind actions subsequently applied on the structure to evaluate its dynamic response, for instance by finite element models of structural systems such as transmission lines [31–33]. These methods allow the representation of the three-dimensional thunderstorm wind field, namely the radial, circumferential and vertical components of the wind velocity as a function of space and time. However, there is still a number of uncertainties associated with the simulation of turbulence [25], the choice of parameters [28,34], and the rules to scale real conditions [35]. In addition, these analyses are burdensome and their results depend on the specific structure dealt with, its position with reference to the centreline of the downdraft, and its orientation; their use in the engineering practice is therefore still rather limited.

The second line, to which this paper belongs, gives up a complete description of the thunderstorm wind field and focuses on the simplified modeling of the most dangerous velocity components for the structure dealt with. In this way, it aims at developing methods for calculating the response of reference models, for instance Single-Degree-Of-Freedom (SDOF) systems and vertical cantilever beams, similar to those formulated for extra-tropical cyclones [2,4–13], so oriented to engineering applications. In this framework, the horizontal component of the wind velocity in the thunderstorm outflows is usually expressed as the sum of a slowly-varying mean part plus a residual zero mean fluctuation dealt with as a non-stationary random process [36–39]. The slowly-varying mean wind velocity is characterized by a vertical "nose" profile that increases up to 50–100 m height, then decreases above; the fluctuation is given by the product of its slowly-varying standard deviation by a rapidly-varying stationary Gaussian random process with zero mean and unit standard deviation. Based on these assumptions, Choi and Hidayat [36] studied first the dynamic response of a point-like SDOF system subjected to a wind velocity field perfectly coherent in space. This study was developed later in [40–42], where the behavior of SDOF systems was analyzed by one parameter, called maximum dynamic magnification factor or dynamic response factor, given by the ratio between the maximum dynamic response and the static response due to the peak wind loading. Kwon and Kareem [43,44] developed a gust front factor framework in which the original gust response factor technique was generalized from stationary to non-stationary wind actions; they provided also a robust interpretation of the conceptual behavior of the structural response. Other authors [45–47] applied advanced techniques using evolutionary spectral densities, wavelet transforms, Galerkin expansions and time-series simulations.

Despite this impressive amount of research, however, there is not yet a model of thunderstorms and their actions on structures that led to a convergence of ideas between scholars and engineers, similar to that which occurred when Davenport formulated his famous model of the dynamic response of structures to synoptic winds. This happens because, on the one hand, the complexity of thunderstorms makes it difficult to formulate physically realistic and simple theories, and, on the other hand, their short duration and small size make the available measurements still rather limited. It follows that wind actions on structures are still almost exclusively determined by the extra-tropical cyclone model that dates back over half a century ago [48], at the most taking the occurrence of thunderstorms into account, if data are available, in the statistical evaluation of the design wind velocity [49,50]. This is not enough, since extra-tropical cyclones and thunderstorms are different phenomena that need separate assessments [18].

This paper is part of a research project that started [18] from the remark that thunderstorms are transient phenomena characterized by short duration, and the structural response to transient phenomena, most notably to earthquakes, is traditionally evaluated by the response spectrum (RS) technique [51,52]. Based on these considerations, a "new" method is here formulated, the Thunderstorm Response Spectrum Technique (TRST), which generalizes the "old" RS technique from earthquakes to thunderstorms. The prospect that this method, though deeply revised and modified, is so very well-known by engineers as to favor its rapid use in both the research and design fields seems to be very attractive.

A previous paper [53] addressed the problem of the thunderstorm response of ideal point-like SDOF systems subjected to wind actions perfectly coherent over the exposed structural surface. The generalization of this method to the thunderstorm response of real space Multi-Degree-Of-Freedom (MDOF) systems involves a crucial aspect. The traditional use of the RS technique is based on the classical model according to which earthquakes give rise to perfectly coherent ground motions at the structural base, and their actions mainly depend on the distribution of the structural masses, namely a property of the mechanical system. Instead, thunderstorms cause partially coherent wind fields that determine wind actions strictly dependent on the wind velocity profile and on the space–time correlation of the fluctuations. Taking a cue from a previous paper by author [54], this major obstacle is overcome by making recourse to the Equivalent Wind Spectrum Technique (EWST) [55,56], a method developed for synoptic stationary winds, the use of which is extended here to non-synoptic non-stationary conditions.

Section 2 develops the wind velocity model subsequently adopted to evaluate the structural response to thunderstorm outflows. Section 3 introduces the basic equations of the dynamic alongwind response of structures to the non-stationary wind velocity model discussed in Section 2; for sake of simplicity, in this stage of the research, they are expressed with reference to a continuous slender vertical cantilever beam, whose response is dominated by the first mode of vibration. Section 4 recalls the fundamentals of the EWST [55,56], and generalizes its use from stationary extra-tropical cyclones to non-stationary thunderstorm outflows. Section 5 formulates the TRST with reference to MDOF systems subjected to partially coherent wind fields; this aim is pursued by introducing the concept of Equivalent RS (ERS), a quantity that multiplied by the peak wind loading furnishes the equivalent static force. Section 6 provides two noteworthy limit solutions that represent upper and lower bounds of the ERS, corresponding to ideal structures with infinitely small and infinitely large surfaces exposed to wind, respectively; it is demonstrated that in these cases the ERS coincides, respectively, with the RS and the base RS (BRS) for SDOF systems developed in [53]. Section 7

formulates a general procedure aimed at assessing the ERS of a thunderstorm record; rules and concepts are also provided in order to evaluate the mean and/or the design ERS. Section 8 extends to MDOF systems a form of parameterization introduced with regard to SDOF systems [53], showing and discussing its most relevant properties and advantages. Section 9 provides a synthesis of the basic steps of the TRST and applies this method to a real structure, highlighting the characteristics that make the TRST particularly suitable for rapid engineering calculations and simple code applications. Section 10 summarizes the main conclusions and draws some prospects for future research advances. Appendix A reports a list of the main symbols, operators and acronyms used in this paper. Appendices B–E illustrate specific aspects.

The application of the TRST provided herein refers, as a case study, to the results of the wind monitoring campaign conducted for the European project "Wind and Ports" [57–59]. Despite this, the method introduced in the present paper is fully general and may be used in any context. Even more it is suitable to be generalized to different types of non-stationary wind phenomena.

2. Wind velocity

In the spirit of simplified analyses aiming to determine the dynamic response of reference structural models to thunderstorm outflows, the horizontal component of the wind velocity is expressed by the classical decomposition rule [36–39,59]:

$$v(z,t) = \bar{v}(z,t) + v'(z,t) \tag{1}$$

where z is the height above ground, $t \in [0, \Delta T]$ is the time, ΔT is an interval between 10 min and 1 h, $\bar{v}$ is the slowly-varying mean wind velocity related to the low frequency harmonic content of v, v' is the residual fluctuation related to the high frequency harmonic content of v. In this paper an over-bar denotes a temporal average. A wide literature exists on the tools aiming to extract $\bar{v}$ from v [38,39,59,60]. Eq. (1) does not consider the change of direction of the wind velocity.

The mean velocity $\bar{v}$ is driven by the large scale flow and is often dealt with as deterministic; the fluctuating velocity is induced by the small scale turbulence and is usually schematized by a non-stationary random process defined as [38]:

$$v'(z,t) = \sigma_v(z,t)\tilde{v}'(z,t) \tag{2}$$

where σ_v is the slowly-varying standard deviation of v', $\tilde{v}'$ is the reduced turbulent fluctuation dealt with as a rapidly-varying stationary Gaussian random field with zero mean and unit standard deviation [39,59]. In this paper the extraction of $\bar{v}$ from v and σ_v from v' is based on a moving average filter, or running-mean [39], with a moving average period $T = 30$ s [59].

Replacing Eq. (2) into Eq. (1), the wind velocity v may be rewritten as:

$$v(z,t) = \bar{v}(z,t)[1 + I_v(z,t)\tilde{v}'(z,t)] \tag{3}$$

where $I_v(z,t) = \sigma_v(z,t)/\bar{v}(z,t)$ is the slowly-varying turbulence intensity [39,59].

The slowly-varying mean wind velocity is expressed as [37,40,43]:

$$\bar{v}(z,t) = \bar{v}_{max}(h)\alpha(z)\gamma(t) \tag{4}$$

where $\bar{v}_{max}$ is the maximum value of $\bar{v}$; h is the height of an anemometer that registers the wind velocity or, more in general, the reference height at which the wind velocity is assigned; α is a non-dimensional function of z that defines the shape of the vertical profile of $\bar{v}$ [27–29,61–65]; γ is a non-dimensional function of t, whose maximum value is $\gamma_{max} = 1$, which expresses the time variation of $\bar{v}$ [30,59,66]. Thus, $\alpha(h) = 1, \bar{v}(h,t) = \bar{v}_{max}(h)\gamma(t)$ and $\bar{v}_{max}(z) = \bar{v}_{max}(h)\alpha(z)$.

Similarly to Eq. (4), the slowly-varying turbulence intensity is expressed here by the relationship:

$$I_v(z,t) = \bar{I}_v(h)\beta(z)\mu(t) \tag{5}$$

where $\bar{I}_v$ is the average value of I_v over ΔT; β is a non-dimensional function of z that defines the shape of the vertical profile of I_v [43]; μ is a non-dimensional function of t that expresses the time variation of I_v [59]. Thus, $\beta(h) = 1, \bar{\mu} = 1, I_v(h,t) = \bar{I}_v(h)\mu(t)$ and $\bar{I}_v(z) = \bar{I}_v(h)\beta(z), \bar{\mu}$ being the average value of μ.

Assuming $\mu(t) = 1$ corresponds to consider I_v as independent of t [43], i.e. $I_v(z,t) = \bar{I}_v(h)\beta(z)$. Assuming $\beta(z) = 1$ corresponds to consider I_v as independent of z, i.e. $I_v(z,t) = \bar{I}_v(h)\mu(t)$; this position seems to be reasonable in proximity of the terrain [59], much more questionable on increasing the height above ground [26]. Assuming $\mu(t) = 1$ and $\beta(z) = 1$ corresponds to consider I_v as independent of both z and t [39–41,67], i.e. $I_v(z,t) = \bar{I}_v(h)$. The dependence of I_v on both z and t is discussed for instance by [68,69].

It is worth noting that the decoupling of space and time in Eqs. (4) and (5) is greatly helpful to the development of simple models of the dynamic response of structures to thunderstorm outflows. In spite of this, it does not reproduce the actual evolution of the wind field [68,70,71]. This topic deserves future research. Author relies on the LiDAR measurements currently undertaken for the European project "Wind, Ports and Sea" [72] may contribute to clarify this point.

The reduced turbulent fluctuation is identified through its cross-power spectral density (CPSD):

$$S_{\tilde{v}'\tilde{v}'}(z,z',n) = \sqrt{S_{\tilde{v}'}(z,n)S_{\tilde{v}'}(z',n)}Coh_{\tilde{v}'\tilde{v}'}(z,z',n) \tag{6}$$

where z' is a height above ground, n is the frequency, $S_{\tilde{v}'}$ and $Coh_{\tilde{v}'\tilde{v}'}$ are, respectively, the power spectral density (PSD) and the coherence function of $\tilde{v}'$ [73,74]. A wide literature supports the possibility of expressing $S_{\tilde{v}'}$ and $Coh_{\tilde{v}'\tilde{v}'}$ by the classical models adopted for synoptic winds [37,39,43,59,70]; a preliminary proposal for using different models was introduced in [38].

Replacing Eqs. (4) and (5) into Eq. (3), the wind velocity may be modeled as:

$$v(z,t) = \bar{v}_{max}(h)\alpha(z)\gamma(t)[1 + \bar{I}_v(h)\beta(z)\mu(t)\tilde{v}'(z,t)] \tag{7}$$

The peak wind velocity $\hat{v}$ is defined as the maximum value of v averaged over a short time interval τ; in this paper $\tau = 1$ s. The quantity $\hat{v}$ is given by the relationship:

$$\hat{v}(z) = \bar{v}_{max}(z)\widehat{G}(z) = \hat{v}(h)\chi(z) \tag{8}$$

where $\widehat{G}$ is a non-dimensional ratio referred to as the peak gust factor [39,59,70], χ is a non-dimensional function of z that defines the shape of the vertical profile of $\hat{v}$ [19,26,70,71]. Dealing with $\widehat{G}$ as independent of z, namely $\widehat{G}(z) = \widehat{G}(h)$, then $\hat{v}(z) = \bar{v}_{max}(z)\widehat{G}(h)$; accordingly, the vertical profiles of $\hat{v}$ and $\bar{v}_{max}$ have the same shape, namely $\chi(z) = \alpha(z)$. This position does not match with the simulations and measurements carried out in [19,71] with reference to a deep stratum of the atmosphere; however, in proximity of the terrain, it agrees with the results reported in [59]. Also this topic deserves more research efforts.

The wind velocity model described above may be made explicit by implementing suitable statistical, analytical or experimental representations of the different ingredients that compose Eq. (7). The TRST has the following properties: (1) $\bar{v}_{max}(h)$ or $\hat{v}(h)$ should be provided by statistical estimates; (2) $\gamma, \mu, \bar{I}_v, \tilde{v}'$ and $\widehat{G}(h)$ are assigned by a wide set of measured thunderstorm velocity records; (3) the use of analytical models is limited, at least in this stage of the research, to define α, β and χ. It is worth noting that, while

many expressions of α have been proposed in literature, no robust expression for β and χ is still available.

The three-dimensional representation of v, not considered in the present paper, will be dealt with in future researches addressed to structures represented by models other than the slender vertical beam. As far as the translational component of the thunderstorm is concerned [37,66,67], not examined here in explicit terms, its possible presence is implicitly taken into consideration by embedding measured thunderstorm records into Eq. (7); this topic deserves future research.

3. Dynamic response

This section provides a general outline of the dynamic response of a structure to a non-stationary wind field, in particular a thunderstorm outflow. This formulation has no direct influence over the assessment of the TRST (Section 5). Nevertheless it is relevant as a reference term of comparison, to support the application of the EWST (Section 4), and to define the bounds of the ERS (Section 6).

Let us consider a MDOF linear system. For sake of simplicity, it is schematized as a continuous slender vertical cantilever beam. This structure is subjected to the alongwind force defined as:

$$f(z,t) = \frac{1}{2}\rho v^2(z,t) b(z) c_D(z) \tag{9}$$

where ρ is the density of air, v is the wind velocity (Eq. (7)), b is the width of the structural surface exposed to wind, c_D is the drag coefficient. Transient aerodynamic effects discussed in [43] are here disregarded for sake of simplicity and for the lack of suitable data; this matter deserves more research efforts.

Let us assume that the structural response to thunderstorm outflows is dominated by the first mode of vibration. Thus, the alongwind displacement is given by:

$$x(z,t) = \psi_1(z) p_1(t) \tag{10}$$

where ψ_1 is the first modal shape and p_1 is the first principal coordinate given by the solution of the differential equation of motion:

$$\ddot{p}_1(t) + 2(2\pi n_1)\xi \dot{p}_1(t) + (2\pi n_1)^2 p_1(t) = \frac{1}{m_1} f_1(t) \tag{11}$$

n_1, ξ, m_1 and f_1 being the first natural frequency, damping coefficient, modal mass and modal force defined as:

$$m_1 = \int_0^H m(z)\psi_1^2(z)dz \tag{12}$$

$$f_1(t) = \int_0^H f(z,t)\psi_1(z)dz \tag{13}$$

where H is the height of the structure and m is its mass per unit length. The hypothesis according to which the structural response depends on the sole first mode of vibration calls for new research with reference to its generalization from synoptic to thunderstorm winds. The analysis of structures schematized by models other than the continuous slender vertical cantilever beam, the evaluation of the structural response by the influence function technique and the role of the higher modes of vibration on the quasi-static part of the response will be the subjects of future studies. Research is also in progress to formulate a new Monte Carlo strategy aiming to simulate thunderstorm wind fields consistent with Eq. (7) and to carry out time-domain analyses of the structural response.

Replacing Eq. (7) into Eq. (9), the wind loading results:

$$f(z,t) = \bar{f}(z,t) + f'(z,t) \tag{14}$$

where $\bar{f}$ and f' are the slowly-varying mean part and the residual fluctuating part of f, respectively. Assuming that the turbulence is small, they are given by:

$$\bar{f}(z,t) = \frac{1}{2}\rho \bar{v}_{max}^2(h)\alpha^2(z)\gamma^2(t) b(z) c_D(z) \tag{15}$$

$$f'(z,t) = \rho \bar{v}_{max}^2(h)\alpha^2(z)\gamma^2(t)\bar{I}_v(h)\beta(z)\mu(t)\tilde{v}'(z,t) b(z) c_D(z) \tag{16}$$

Replacing Eqs. (14)–(16) into Eq. (13), the first modal force is given by:

$$f_1(t) = \bar{f}_1(t) + f_1'(t) \tag{17}$$

where $\bar{f}_1$ and f_1' are the slowly-varying mean part and the residual fluctuating part of f_1, respectively:

$$\bar{f}_1(t) = \frac{1}{2}\rho \bar{v}_{max}^2(h) a_1 \gamma^2(t) \tag{18}$$

$$f_1'(t) = \rho \bar{v}_{max}^2(h) a_1 \gamma^2(t)\bar{I}_v(h)\mu(t)\tilde{a}_1'(t) \tag{19}$$

a_1 is dimensionally an area, $\tilde{a}_1'$ is a non-dimensional function of t:

$$a_1 = \int_0^H \alpha^2(z) b(z) c_D(z)\psi_1(z)dz \tag{20}$$

$$\tilde{a}_1'(t) = \frac{1}{a_1}\int_0^H \alpha^2(z)\beta(z)\tilde{v}'(z,t) b(z) c_D(z)\psi_1(z)dz \tag{21}$$

Replacing Eq. (17) into Eq. (11), the first principal coordinate is given by:

$$p_1(t) = \bar{p}_1(t) + p_1'(t) \tag{22}$$

where $\bar{p}_1$ and p_1' are the components of p_1 due to the slowly-varying mean part (Eqs. (15) and (18)) and to the residual fluctuating part (Eqs. (16) and (19)) of the wind loading, respectively.

The slowly-varying mean part of p_1 is given by:

$$\bar{p}_1(t) = \frac{1}{2}\rho \bar{v}_{max}^2(h) a_1 A_1(t) \tag{23}$$

where

$$A_1(t) = \int_0^t h_1(t-\tau)\gamma^2(\tau)d\tau \tag{24}$$

h_1 being the impulse response function of p_1:

$$h_1(t) = e^{-\xi(2\pi n_1)t}\frac{1}{m_1(2\pi n_1)\sqrt{1-\xi^2}}\sin\left(2\pi n_1\sqrt{1-\xi^2}t\right) \tag{25}$$

The residual fluctuating part of p_1 may be evaluated remembering that γ and μ are slowly-varying functions of time, while $\tilde{v}'$ and $\tilde{a}_1'$ are rapidly-varying stationary Gaussian random processes [59]. So, p_1' may be regarded as a uniformly modulated random process [75] whose evolutionary spectral density is given by [76]:

$$S_{p_1'}(n,t) = [\rho \bar{v}_{max}^2(h) a_1 \bar{I}_v(h)]^2 |A_1'(n,t)|^2 S_{\tilde{a}_1'}(n) \tag{26}$$

where

$$A_1'(n,t) = \int_0^t h_1(t-\tau)\gamma^2(\tau)\mu(\tau)e^{-i(2\pi n)(t-\tau)}d\tau \tag{27}$$

i is the imaginary unit, $S_{\tilde{a}_1'}$ is the PSD of $\tilde{a}_1'$ (Eq. (21)):

$$S_{\tilde{a}_1'}(n) = \frac{1}{a_1^2}\int_0^H\int_0^H \alpha^2(z)\alpha^2(z')\beta(z)\beta(z')S_{\tilde{v}'\tilde{v}'}(z,z',n) b(z) b(z') c_D(z) c_D(z')\psi_1(z)\psi_1(z')dzdz' \tag{28}$$

$S_{\tilde{v}'\tilde{v}'}$ is the CPSD of $\tilde{v}'$ (Eq. (6)). Eq. (27) points out the modulating role of μ [59]; it is usually disregarded in literature, assuming $\mu = 1$ [36–47].

Appendix B provides simplified expressions of Eqs. (24) and (27). The distribution of the maximum value of p_1 is reported for instance in [77].

4. Equivalent wind spectrum technique

The EWST, introduced in [55] and perfected in [56] for slender structures, is a method that drastically reduces the computational burden for evaluating the wind-induced response to stationary synoptic winds. It consists in replacing the actual turbulent fluctuation, as a random function of time and space, by an equivalent turbulent fluctuation, as a random function of time identically coherent in space. This quantity is defined in such a way that the aerodynamic admittance associated with it matches, in the best possible way, that involved by the actual turbulence field.

In order to apply the EWST to non-stationary thunderstorm outflows, the coherence function of the reduced turbulent fluctuation $\tilde{v}'$ (Eq. (6)) is expressed by:

$$Coh_{\tilde{v}'\tilde{v}'}(z,z',n) = \exp\left\{-\frac{2nc_z|z-z'|}{\bar{v}_{max}(z)+\bar{v}_{max}(z')}\right\} \tag{29}$$

where c_z is the exponential decay coefficient of $\tilde{v}'$ along z. The conventional choice of identifying the slowly-varying mean wind velocity with its maximum value calls for future analyses. It is worth noting that the application of the EWST does not require any explicit hypothesis on the PSD of $\tilde{v}'$.

Based on Eq. (29), the reduced equivalent turbulent fluctuation $\tilde{v}'_{eq}$ is defined through its PSD:

$$S_{\tilde{v}',eq}(n,\delta) = S_{\tilde{v}'}(z_{eq},n)C(\delta n) \tag{30}$$

where $S_{\tilde{v}'}$ is the PSD of $\tilde{v}'$, z_{eq} is an appropriate equivalent height, C is a frequency filter that takes into account the coherence of $\tilde{v}'$ (Eq. (29)) by reducing its PSD in equivalent terms:

$$C(\eta) = \frac{1}{\eta} - \frac{1}{2\eta^2}(1-e^{-2\eta}) \quad (\eta > 0); \quad C(0) = 1 \tag{31}$$

η is the argument of the operator C, δ is a length referred to as the size factor:

$$\delta = \frac{\kappa c_z H}{\bar{v}_{max}(z_{eq})} \tag{32}$$

in which κ is a non-dimensional coefficient referred to as the modal shape factor.

Dealing with synoptic winds and slender vertical cantilever structures whose first modal shape may be approximated as $\psi_1(z) = (z/H)^{\zeta}$, the equivalent height and the modal shape factor are given by [56]:

$$z_{eq} = 0.6H; \quad \kappa = \frac{0.5}{(\zeta+1)^{0.55}} \tag{33}$$

A preliminary parametric numerical analysis was carried out on varying the wind and the structural properties; in particular, different shapes of the "nose" profile were investigated on changing the height of the structure. Outcomes seem to show that Eq. (33) provides enough suitable results also for thunderstorms. More systematic analyses are currently in progress to validate or improve the above expressions. Appendix C illustrates the application of the EWST throughout an example.

Adopting the above definition of $\tilde{v}'_{eq}$, Eq. (7) may be rewritten as:

$$v_{eq}(z,t,\delta) = \bar{v}_{max}(h)\alpha(z)\gamma(t)[1+\bar{I}_v(h)\beta(z)\mu(t)\tilde{v}'_{eq}(t,\delta)] \tag{34}$$

where v_{eq} is referred to as the equivalent wind velocity; this quantity is expressed as an explicit function of δ in order to stress the key role of this parameter. This new definition of the wind velocity does not modify the slowly-varying mean part of the force (Eq. (15)), of the first modal force (Eq. (18)) and of the first principal coordinate (Eq. (23)). Instead, it drastically changes their residual fluctuating parts (Eqs. (16), (19) and (26)) as follows:

$$f'(z,t,\delta) = \rho\bar{v}^2_{max}(h)\alpha^2(z)\gamma^2(t)\bar{I}_v(h)\beta(z)\mu(t)\tilde{v}'_{eq}(t,\delta)b(z)c_D(z) \tag{35}$$

$$f'_1(t,\delta) = \rho\bar{v}^2_{max}(h)a_1\gamma^2(t)\bar{I}_v(h)\mu(t)\tilde{v}'_{eq}(t,\delta) \tag{36}$$

$$S_{p'_1}(n,t,\delta) = [\rho\bar{v}^2_{max}(h)a_1\bar{I}_v(h)]^2|A'_1(n,t)|^2 S_{\tilde{v}',eq}(n,\delta) \tag{37}$$

The comparison between Eqs. (19) and (36) and Eqs. (26) and (37) emphasizes the following properties:

$$\tilde{a}'_1(t) = \tilde{v}'_{eq}(t,\delta) \tag{38}$$

$$S_{\tilde{a}'_1}(n) = S_{\tilde{v}',eq}(n,\delta) \tag{39}$$

Eqs. (38) and (39) represent formidable simplifications of Eqs. (21) and (28). Moreover, they support the application of the EWST to non-stationary thunderstorm outflows, since this method strictly operates on the sole stationary part of the turbulent fluctuations.

5. Response spectrum technique

This section provides the fundamentals of the TRST by focusing on three aspects: (1) the extension of the procedure developed in [53] from an ideal point-like SDOF system to an actual space MDOF system, schematized herein as a continuous slender vertical cantilever beam; (2) the comparison with the more classical theory developed in Section 3; (3) the use of the EWST (Section 4) as a basic tool. In this preliminary stage of the research two simplified hypotheses on the wind velocity are used, whose properties are discussed in Section 2: (1) the turbulence intensity I_v is independent of the height z above ground, namely $\beta = 1$ in Eq. (5); (2) the vertical profile of the peak wind velocity $\hat{v}$ (Eq. (8)) has the same shape of the vertical profile of the slowly-varying mean wind velocity $\bar{v}$ (Eq. (4)), namely $\chi = \alpha$. Research is in progress to generalize the following formulation by overcoming these two limitations.

Based upon Eq. (9) with $\chi = \alpha$, the peak wind force induced by thunderstorm outflows is given by:

$$\hat{f}(z) = \frac{1}{2}\rho\hat{v}^2(h)\alpha^2(z)b(z)c_D(z) \tag{40}$$

Accordingly, the peak static displacement is given by:

$$\hat{x}(z) = \frac{1}{m_1(2\pi n_1)^2}\frac{1}{2}\rho\hat{v}^2(h)a_1\psi_1(z) \tag{41}$$

Let us introduce the reduced equivalent wind velocity defined as:

$$u_{eq}(t,\delta) = \frac{v_{eq}(h,t,\delta)}{\hat{v}(h)} \tag{42}$$

where v_{eq} is given by Eq. (34) with $\beta = 1$. Accordingly, the wind force provided by Eq. (9) results:

$$f(z,t) = \frac{1}{2}\rho\hat{v}^2(h)\alpha^2(z)u^2_{eq}(t,\delta)b(z)c_D(z) \tag{43}$$

The first modal force given by Eq. (13) may be rewritten as:

$$f_1(t) = \frac{1}{2}\rho\hat{v}^2(h)a_1u^2_{eq}(t,\delta) \tag{44}$$

The equation of motion defined by Eq. (11) assumes the form:

$$\ddot{p}_1(t) + 2(2\pi n_1)\xi\dot{p}_1(t) + (2\pi n_1)^2 p_1(t) = \frac{1}{m_1}\frac{1}{2}\rho\hat{v}^2(h)a_1 u_{eq}^2(t,\delta) \tag{45}$$

It is worth noting that, differently from Eqs. (16), (19) and (26), Eqs. (43)–(45) do not call for assuming that the turbulence is small. On the other hand, differently from Eqs. (43)–(45), Eqs. (16), (19) and (26) do not call for assuming that the turbulence intensity is independent of height.

Let us introduce the reduced equivalent displacement defined as:

$$d_{eq}(t) = \frac{x(z,t)}{\hat{x}(z)} = \frac{2m_1(2\pi n_1)^2}{\rho\hat{v}^2(h)a_1}p_1(t) \tag{46}$$

This quantity is independent of z since the structural response depends on the sole first mode of vibration. By virtue of Eq. (46), d_{eq} is given by the solution of the differential equation of motion:

$$\ddot{d}_{eq}(t) + 2\xi(2\pi n_1)\dot{d}_{eq}(t) + (2\pi n_1)^2 d_{eq}(t) = (2\pi n_1)^2 u_{eq}^2(t,\delta) \tag{47}$$

Paraphrasing the definition of the thunderstorm RS, S_d, introduced in [53] for a point-like SDOF system, the thunderstorm ERS for a vertical MDOF system is defined as:

$$S_{d,eq} = d_{eq,max} \tag{48}$$

where $d_{eq,max}$ is the maximum value of d_{eq} (Eq. (47)). It is worth noting that the RS S_d of a point-like SDOF system subjected to a perfectly coherent wind field depends on the wind velocity v, scaled by the peak wind velocity $\hat{v}$, and on two parameters: the fundamental frequency n_0 and the damping coefficient ξ. Eqs. (47) and (48) show that the ERS of a vertical MDOF system subjected to a partially coherent wind field depends on one more parameter, the size factor δ, that synthesizes the role of the aerodynamic admittance; of course, n_1 replaces n_0.

Thanks to the linearity of the structure, the maximum displacement and the equivalent static force result:

$$x_{max}(z) = \hat{x}(z)\cdot S_{d,eq} \tag{49}$$

$$f_{eq}(z) = \hat{f}(z)\cdot S_{d,eq} \tag{50}$$

where x_{max} is the maximum value of x (Eq. (10)), and f_{eq} is the force that statically applied on the structure causes x_{max}.

Table 1 shows a comparison between the TRST for a point-like SDOF system subjected to a fully coherent wind field and a vertical MDOF system subjected to a partially coherent wind field. The equation numbers for the point-like SDOF system are those utilized in [53]. The equation numbers for the vertical MDOF system are those utilized in the present paper.

6. Upper and lower bounds

Section 7 provides a general framework for solving Eq. (47) and determining the ERS of a vertical MDOF system (Eq. (48)). Before introducing this framework, however, this section shows that Eq. (48) admits two noteworthy limit solutions that represent, respectively, an upper and a lower bound of the ERS. Both these bounds correspond to solutions already derived in [53] with reference to a point-like SDOF system.

The upper bound corresponds to the ideal case in which the wind field is perfectly coherent, or the structural surface exposed to wind is infinitely small, or the aerodynamic admittance is unit. This is equivalent to assume $\delta = 0$ (Eq. (32)) and $C = 1$ (Eq. (31)). Thus (Eq. (30)):

$$S_{\tilde{v}',eq}(n,\delta) = S_{\tilde{v}',eq}(n,0) = S_{\tilde{v}'}(z_{eq},n) \tag{51}$$

Since in this stage of the research single velocity records have been mainly analyzed [59] and few high-resolution vertical velocity profiles are still available [72], the PSD of $\tilde{v}'$ at the equivalent height z_{eq} is identified with the PSD of $\tilde{v}'$ at the height h of the anemometer. Accordingly, the reduced equivalent turbulence fluctuation results:

$$\tilde{v}'_{eq}(t,\delta) = \tilde{v}'_{eq}(t,0) = \tilde{v}'(h,t) \tag{52}$$

Eq. (52) corresponds to assuming that the PSD of $\tilde{v}'$ is independent of z. This is not fully consistent with the results provided in [59], according to which $S_{\tilde{v}'}$ may be expressed as a function of $\tilde{n} = nz/\bar{v}_{max}(z)$, so it implicitly depends on z. While waiting to collect more data and to carry out new analyses, this shortcoming is overcome in Section 8 through a different parameterization.

Based on this model, the equivalent wind velocity v_{eq} (Eq. (34)) identifies itself with the wind velocity v (Eq. (7)) at $z = h$. Consequently, the reduced equivalent wind velocity u_{eq} (Eq. (42)) identifies itself with the reduced wind velocity u introduced in [53] for a point-like SDOF system (Table 1), namely:

$$u_{eq}(t,\delta) = u_{eq}(t,0) = \frac{v_{eq}(h,t,0)}{\hat{v}(h)} = \frac{v(h,t)}{\hat{v}(h)} = u(t) \tag{53}$$

Thus, d_{eq} (Eq. (47)) identifies itself with the reduced displacement d given by the solution of the differential equation of motion:

$$\ddot{d}(t) + 2\xi(2\pi n_1)\dot{d}(t) + (2\pi n_1)^2 d(t) = (2\pi n_1)^2 u^2(t) \tag{54}$$

It follows that the ERS $S_{d,eq}$ of a vertical MDOF system (Eq. (48)) identifies itself with the RS S_d of a point-like SDOF system, namely:

$$S_{d,eq} = S_d = d_{max} \tag{55}$$

where d_{max} is the maximum value of d.

The lower bound corresponds to the ideal case in which the wind field is fully incoherent, or the structural surface exposed to

Table 1
Comparison between the TRST for point-like SDOF systems and vertical MDOF systems.

Point-like SDOF systems		Vertical MDOF systems	
Equation	Number[a]	Equation	Number
$\hat{f} = \frac{1}{2}\rho\hat{v}^2 A c_D$	(34)	$\hat{f}(z) = \frac{1}{2}\rho\hat{v}^2(h)\alpha^2(z)b(z)c_D(z)$	(40)
$\hat{x} = \frac{1}{m(2\pi n_0)^2}\frac{1}{2}\rho\hat{v}^2 A c_D$	(35)	$\hat{x}(z) = \frac{1}{m_1(2\pi n_1)^2}\frac{1}{2}\rho\hat{v}^2(h)a_1\psi_1(z)$	(41)
$u(t) = \frac{v(t)}{\hat{v}}$	(36)	$u_{eq}(t,\delta) = \frac{v_{eq}(h,t,\delta)}{\hat{v}(h)}$	(42)
$d(t) = \frac{x(t)}{\hat{x}}$	(37)	$d_{eq}(t) = \frac{x(z,t)}{\hat{x}(z)}$	(46)
$\ddot{d}(t) + 2\xi(2\pi n_0)\dot{d}(t) + (2\pi n_0)^2 d(t) = (2\pi n_0)^2 u^2(t)$	(20)	$\ddot{d}_{eq}(t) + 2\xi(2\pi n_1)\dot{d}_{eq}(t) + (2\pi n_1)^2 d_{eq}(t) = (2\pi n_1)^2 u_{eq}^2(t,\delta)$	(47)
$S_d = d_{max}$	(21)	$S_{d,eq} = d_{eq,max}$	(48)
$x_{max} = \hat{x}\cdot S_d$	(38)	$x_{max}(z) = \hat{x}(z)\cdot S_{d,eq}$	(49)
$f_{eq} = \hat{f}\cdot S_d$	(39)	$f_{eq}(z) = \hat{f}(z)\cdot S_{d,eq}$	(50)

[a] Equation numbers for point-like SDOF systems refer to [53]. In this case, A is the area of the surface exposed to wind, m is the mass, the RS identifies with the reduced peak RS, namely $S_d = S_d^{\wedge}$.

wind is infinitely large, or the aerodynamic admittance is null. This is equivalent to assume $\delta \to \infty$ (Eq. (32)) and $C = 0$ (Eq. (31)). Thus (Eq. (30)):

$$S_{\tilde{v}',eq}(n,\delta) = S_{\tilde{v}',eq}(n,\infty) = 0 \tag{56}$$

Accordingly, the reduced equivalent turbulence fluctuation is given by:

$$\tilde{v}'_{eq}(t,\delta) = \tilde{v}'_{eq}(t,\infty) = 0 \tag{57}$$

Based on this model, the equivalent wind velocity v_{eq} (Eq. (34)) identifies itself with the slowly-varying mean wind velocity $\bar{v}$ (Eq. (4)) at $z = h$. Consequently, the reduced equivalent wind velocity u_{eq} (Eq. (42)) identifies itself with the reduced slowly-varying mean wind velocity $\bar{u}$ introduced in [53] for a point-like SDOF system, namely:

$$u_{eq}(t,\delta) = u_{eq}(t,\infty) = \frac{v_{eq}(h,t,\infty)}{\hat{v}(h)} = \frac{\bar{v}(h,t)}{\hat{v}(h)} = \bar{u}(t) \tag{58}$$

Thus, d_{eq} (Eq. (47)) identifies itself with the reduced mean displacement $\bar{d}$ given by:

$$\bar{d}(t) = \bar{u}^2(t) \tag{59}$$

It follows that the ERS $S_{d,eq}$ of a vertical MDOF system (Eq. (48)) identifies itself with the RS of a point-like SDOF system submitted to the slowly-varying mean wind velocity $\bar{v}$. This quantity was called in [53] the BRS and was denoted by S_{db}; accordingly:

$$S_{d,eq} = S_{db} = \bar{d}_{max} = \frac{1}{\hat{G}^2(h)} \tag{60}$$

where $\bar{d}_{max}$ is the maximum value of $\bar{d}$.

Using together Eqs. (55) and (60), the actual value of $S_{d,eq}$ has the following property:

$$S_{db} \leqslant S_{d,eq} \leqslant S_d \tag{61}$$

Fig. 1 provides a qualitative representation of the trend depicted above. The anomalous condition occurring for unrealistically low natural frequencies was explained in [53].

7. Equivalent response spectrum

The assessment of the ERS (Eq. (48)) is one of the most typical features of the TRST: it involves the joint numerical processing of a thunderstorm record and the implementation of an analytical model that conceptually reconstructs the complete wind field around the measured data. Keeping in mind the results obtained in Sections 5 and 6, the following procedure is formulated.

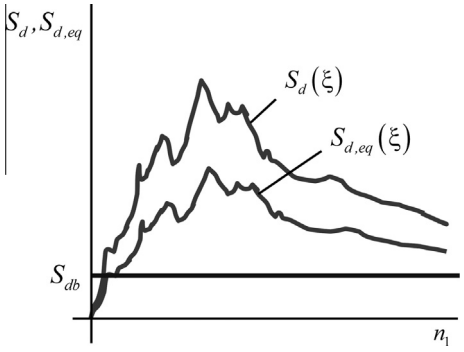

Fig. 1. General trend of the thunderstorm ERS.

(1) Consider the wind velocity $v(h,t)$ recorded during a thunderstorm by an anemometer at the height $z = h$, apply the decomposition rule provided by Eq. (7) with $\alpha(h) = \beta(h) = 1$, and extract from it the reduced turbulent fluctuation $\tilde{v}'(h,t)$ and the peak wind velocity $\hat{v}(h)$.

(2) Evaluate the Fourier transform of $\tilde{v}'(h,t)$, namely $\tilde{V}'(h,n) = F\{\tilde{v}'(h,t)\}$, after making the signal compatible with the execution of this operation [78].

(3) Evaluate the Fourier transform of the reduced equivalent turbulent fluctuation $\tilde{v}'_{eq}(t,\delta)$ by the method described in Appendix D:

$$\tilde{V}'_{eq}(n,\delta) = \tilde{V}'(h,n)\sqrt{C(\delta n)} \tag{62}$$

$\delta = \delta_j$ ($j = 1,2,\ldots,J$) (Eq. (32)) being a set of J values of the size factor that represent all the real cases.

(4) Evaluate $\tilde{v}'_{eq}(t,\delta)$ as the inverse Fourier transform of $\tilde{V}'_{eq}(n,\delta)$, namely $\tilde{v}'_{eq}(t,\delta) = F^{-1}\{\tilde{V}'_{eq}(n,\delta)\}$, being $\delta = \delta_j$ ($j = 1,2,\ldots,J$).

(5) Replace $\tilde{v}'_{eq}(t,\delta)$ into Eq. (34) with $\alpha(h) = \beta(h) = 1$, and determine the equivalent wind velocity $v_{eq}(h,t,\delta)$, being $\delta = \delta_j$ ($j = 1,2,\ldots,J$).

(6) Replace $v_{eq}(h,t,\delta)$ into Eq. (42), and determine the reduced equivalent wind velocity $u_{eq}(t,\delta)$, being $\delta = \delta_j$ ($j = 1,2,\ldots,J$).

(7) Replace $u_{eq}(t,\delta)$ into Eq. (47), and determine the reduced displacement $d_{eq}(t)$, being $\delta = \delta_j$ ($j = 1,2,\ldots,J$), for a set of L values of the first natural frequency $n_1 = n_{11}$ ($l = 1,2,\ldots,L$) and M values of the damping coefficient $\xi = \xi_m$ ($m = 1,2,\ldots,M$) that represent all the real cases.

(8) Apply Eq. (48), and determine the ERS, $S_{d,eq}$, being $\delta = \delta_j$ ($j = 1,2,\ldots,J$), $n_1 = n_{11}$ ($l = 1,2,\ldots,L$) and $\xi = \xi_m$ ($m = 1,2,\ldots,M$).

Fig. 2 illustrates some steps of this procedure. Scheme (a) shows the velocity $v(h,t)$ recorded by anemometer 3 of the Port of La Spezia ($h = 10$ m) during the thunderstorm occurred on 25 October 2011. Scheme (b) shows the reduced turbulent fluctuation $\tilde{v}'(h,t)$; it coincides with the reduced equivalent turbulent fluctuation $\tilde{v}'_{eq}(t,\delta) = \tilde{v}'_{eq}(t,0)$ and corresponds to the upper bound in which the turbulence field is perfectly coherent or the structural surface is infinitely small (Section 6). Schemes (c) and (d) show the reduced equivalent turbulent fluctuation $\tilde{v}'_{eq}(t,\delta)$ for $\delta = 1$ and 20 m, respectively; on increasing δ the high frequency harmonic content of $\tilde{v}'_{eq}$ reduces (Section 4); this reproduces, in equivalent terms, the role of the aerodynamic admittance related to the partial coherence of the turbulence field. Schemes (e) and (f) show the reduced equivalent velocity $v_{eq}(h,t,\delta)$ for $\delta = 1$ and 20 m, respectively; on increasing δ the signals approach the slowly-varying mean wind velocity $\bar{v}(h,t)$ that represents the limit of $v_{eq}(h,t,\delta)$ for δ tending to infinite; this corresponds to the lower bound in which the turbulence field is fully incoherent, or the structural surface is infinitely large (Section 6).

According to the definition given in [53], a set of thunderstorm records is said to be homogeneous provided that their properties relevant to determining the RS are characterized by non-quantifiable uncertainties. The reader is addressed to [53] for a detailed discussion on this delicate topic.

Let us consider a set of N homogeneous thunderstorm records $v(h,t) = v_i(h_i,t)$ ($i = 1,2,\ldots,N$) and their ERS $S_{d,eq} = S_{di,eq}$ ($i = 1,2,\ldots,N$); h_i is the height of the anemometer that detects the ith record. The mean value, the standard deviation (std) and the coefficient of variation (cov) of the ERS are given by:

$$\langle S_{d,eq} \rangle = \frac{1}{N}\sum_{i=1}^{N} S_{di,eq} \tag{63}$$

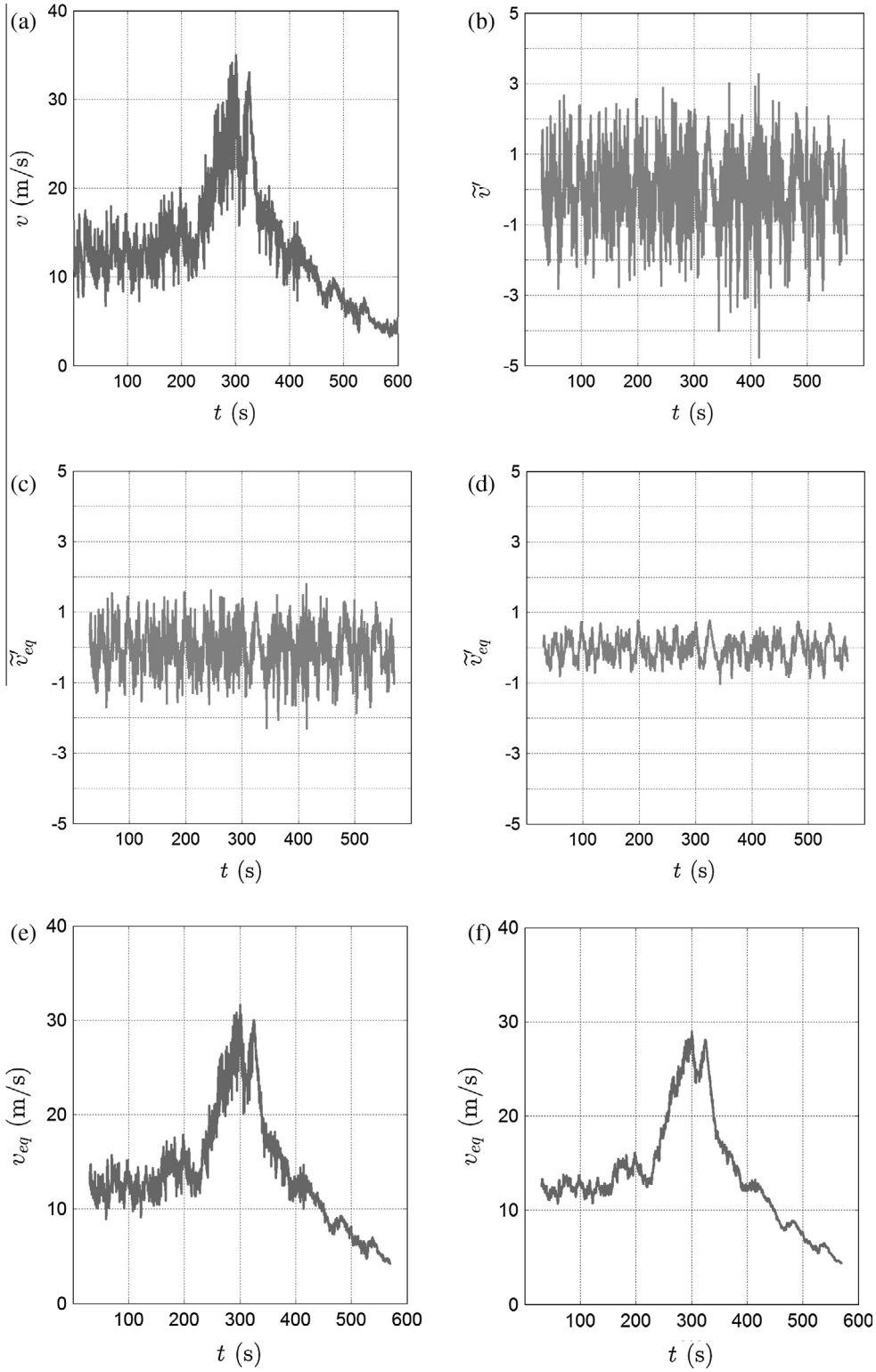

Fig. 2. (a) Thunderstorm wind velocity record; (b) reduced turbulent fluctuation; reduced equivalent turbulent fluctuation for $\delta = 1$ m (c) and $\delta = 20$ m (d); equivalent wind velocity for $\delta = 1$ m (e) and $\delta = 20$ m (f).

$$std(S_{d,eq}) = \frac{1}{N}\sqrt{\sum_{i=1}^{N}(S_{di,eq} - \langle S_{d,eq}\rangle)^2} \tag{64}$$

$$cov(S_{d,eq}) = \frac{std(S_{d,eq})}{\langle S_{d,eq}\rangle} \tag{65}$$

However, a problem highlighted in [53] is still open and committed for future researches currently in progress: what is the best choice of the thunderstorm design ERS to adopt in Eqs. (49) and (50)? Is the mean value of the ERS representative of the design ERS of a set of thunderstorm records? Or is it better to use its mean

value plus one *std* as often done in seismic engineering? Or is even better to resort, and how, to suitably defined exceedance probability levels of the ERS?

Fig. 3 shows the mean ERS of 93 thunderstorm records detected in the Ports of Genoa, La Spezia and Livorno in the period 2011–2012 [53,59]. The variation of n_1 is extended until unrealistic values to show the general trend and the limit tendencies of the ERS. Schemes (a)–(e) refer, respectively, to the damping coefficients $\xi = 0.002, 0.005, 0.01, 0.02, 0.05$. Each scheme provides the mean ERS as a function of the first natural frequency n_1, on varying the size factor in the range $\delta = 0.1$–200 m; it diminishes on increasing both ξ and δ. The upper diagram ($\delta = 0$) refers to the upper bound (Eq. (55)); the lower diagram ($\delta \to \infty$) refers to the lower bound (Eq. (60)).

It is worth noting that the RS of a point-like SDOF system is almost independent of the fundamental frequency n_0, at least in the range of its most typical values [53]. This situation does not radically vary, but seems to be less apparent, for the ERS of a vertical MDOF system; this happens because the aerodynamic admittance reduces faster the high frequency harmonic content of the structural response, the greater is the structural surface exposed to wind, thus the size factor δ. It follows that, on the one hand,

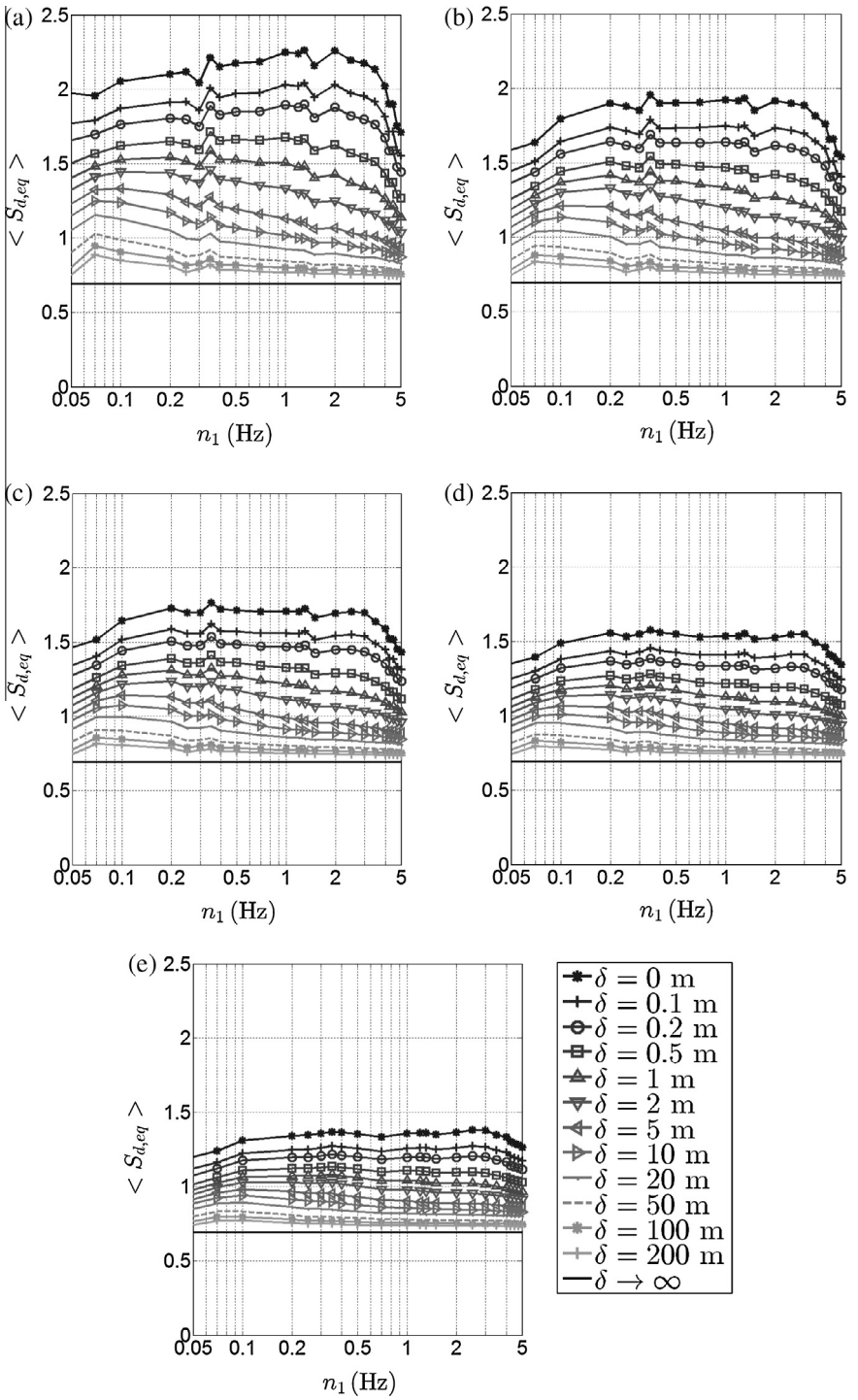

Fig. 3. Mean ERS as a function of n_1 and δ for: (a) $\xi = 0.002$; (b) $\xi = 0.005$; (c) $\xi = 0.01$; (d) $\xi = 0.02$; (e) $\xi = 0.05$.

one of the major advantages of parameterizing the RS as a function of n_1 is definitely weaker; on the other hand, one of the most peculiar aspects of synoptic winds is partly recovered, at least in the most typical range of the n_1, ξ and δ values: the structural response reduces on increasing the natural frequency. In the case of thunderstorms, however, this trend seems to be less evident than that which occurs for synoptic winds [18]. This topic deserves further research.

Fig. 4 completes the information in Fig. 3 by showing, in an analogous format, the *cov* of the ERS. This quantity diminishes on increasing ξ and tends to diminish on increasing n_1. In addition, it gradually changes from $\delta = 0$ to $\delta \to \infty$; however, differently from Fig. 3, where $\langle S_{d,eq} \rangle$ diminishes on increasing δ, the dependence of $cov(S_{d,eq})$ on δ is not monotonic. This remark agrees with the trends pointed out in [53]. The large *cov* values in the low frequency range do not correspond to realistic cases [53].

8. Parameterized equivalent response spectrum

The RS of a point-like SDOF system assumes different shapes depending on whether it is expressed as a function of n_0 or of its reduced value $\tilde{n}_0 = n_0 z / \bar{v}_{max}$ [53]. Remembering that expressing

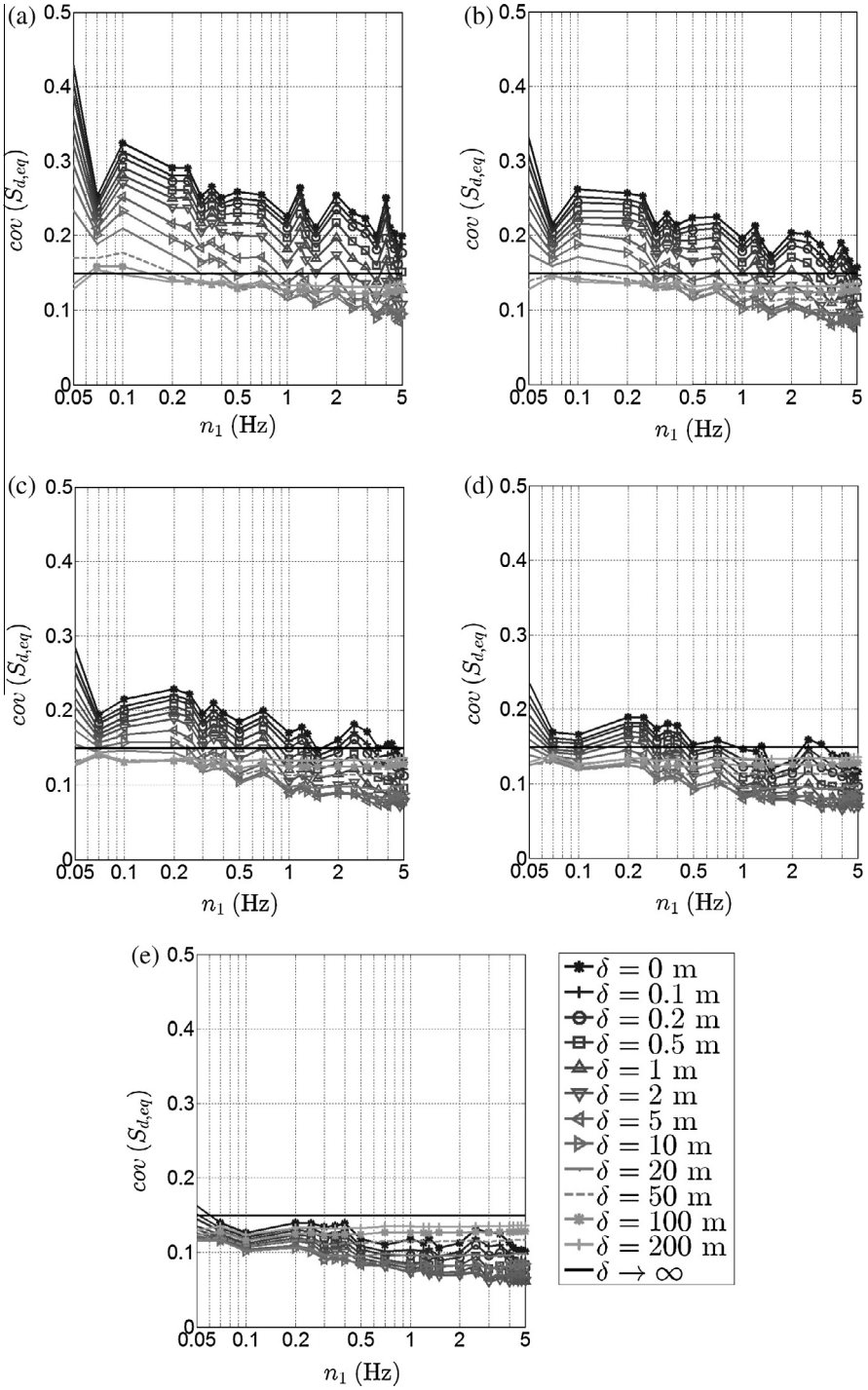

Fig. 4. *Cov* of the ERS as a function of n_1 and δ for: (a) $\xi = 0.002$; (b) $\xi = 0.005$; (c) $\xi = 0.01$; (d) $\xi = 0.02$; (e) $\xi = 0.05$.

$\langle S_{d,eq} \rangle$ as a function of n_1 (MDOF systems) does not imply the same advantages of expressing $\langle S_d \rangle$ as a function of n_0 (SDOF systems) (Section 7), this section investigates the consequences of parameterizing the ERS as a function of suitably reduced values of n_1 and δ. The following choices are adopted:

$$\tilde{n}_1 = \frac{n_1 z_{eq}}{\bar{v}_{max}(z_{eq})} \tag{66}$$

$$\tilde{\delta} = \frac{\kappa C_z H}{z_{eq}} \tag{67}$$

where $\tilde{n}_1$ and $\tilde{\delta}$ are, respectively, the reduced first natural frequency and the reduced size factor.

Based upon the above definitions, and paraphrasing the method developed in [53], Eq. (47) may be conveniently rewritten as:

$$\ddot{d}_{eq}(\tilde{t}) + 2\xi(2\pi\tilde{n}_1)\dot{d}_{eq}(\tilde{t}) + (2\pi\tilde{n}_1)^2 d_{eq}(\tilde{t}) = (2\pi\tilde{n}_1)^2 u_{eq}^2(\tilde{t}, \tilde{\delta}) \tag{68}$$

where $\tilde{t} = t\bar{v}_{max}(z_{eq})/z_{eq}$ is the reduced time, $u_{eq}(\tilde{t}, \tilde{\delta})$ is the reduced equivalent wind velocity (Eq. (42)). Accordingly, the reduced equivalent turbulent fluctuation $\tilde{v}'_{eq}(\tilde{t}, \tilde{\delta})$ is identified by its PSD:

$$S_{\tilde{v}',eq}(\tilde{n}, \tilde{\delta}) = S_{\tilde{v}'}(z_{eq}, \tilde{n}) C(\tilde{\delta}\tilde{n}) \tag{69}$$

$\tilde{n} = nz_{eq}/\bar{v}_{max}(z_{eq})$ being the reduced frequency. These definitions imply three relevant aspects.

First, the above formulation overcomes the previous shortcoming according to which the PSD of $\tilde{v}'$ is independent of z (Sections 5 and 6). Under this point of view, the TRST returns to be consistent with the results obtained in [59], according to which the PSD of $\tilde{v}'$ may be parameterized as a function of $nz/\bar{v}_{max}(z)$; in this case, $z = z_{eq}$.

Second, differently from the size factor δ (Eq. (32)), namely a length that may assume a broad band of values, the reduced size factor $\tilde{\delta}$ (Eq. (67)) is a non-dimensional quantity whose value usually falls in a restricted domain. In particular, dealing with slender vertical cantilever structures, $\zeta = 0.7–2.5$; $z_{eq}/H = 0.6$ and $\kappa = 0.25–0.37$ (Eq. (33)); $c_z = 7 - 15$ [73]. Thus, $\tilde{\delta} = 3 - 9$.

Third, Eq. (47) may be regarded as a particular case of Eq. (68), obtained assuming $\tilde{t} = t, \tilde{n}_1 = n_1$ and $\tilde{\delta} = \delta$. Thus, Eq. (68) represents a unitary equation of motion from which the two forms of parameterization defined above can be obtained through a suitable and unique numeric integration algorithm. Appendix E provides a synthetic generalization of the procedure developed in Section 7.

Fig. 5 shows the mean ERS of the 93 thunderstorm records used to obtain Fig. 3 as a function of $\tilde{n}_1$ on varying $\tilde{\delta}$; schemes (a)–(e) refer, respectively, to $\xi = 0.002$, 0.005, 0.01, 0.02, 0.05. As in Fig. 3, the mean ERS reduces on increasing both ξ and $\tilde{\delta}$. The upper diagram ($\tilde{\delta} = 0$) corresponds to the upper bound (Eq. (55)); the lower diagram ($\tilde{\delta} \to \infty$) corresponds to the lower bound (Eq. (60)). Fig. 6 completes the information given by Fig. 5 showing, in an analogous format, the *cov* of the ERS.

Figs. 5 and 6 point out a relevant aspect: at least for slender vertical structures, the values assumed by $\tilde{\delta}$ belong to a so restricted range as to make $\langle S_{d,eq} \rangle$ and $cov(S_{d,eq})$ almost independent of this parameter. Under this viewpoint, it is intriguing to assign $\tilde{\delta}$ one value on average representative of the behavior of all the slender vertical structures. To this aim, let us assume $c_z = 10$, $\zeta = 2$, $z_{eq} = 0.6$-H and $\kappa = 0.27$ (Eq. (33)); thus, $\tilde{\delta} = 4.5$ (Eq. (67)). In this case, like the mean value and the *cov* of the RS for a point-like SDOF system, also the mean value and the *cov* of the ERS for a vertical MDOF system depend on only two parameters: $\tilde{n}_1$ and ξ. Adopting this new conception, Figs. 5 and 6 are replaced by the couple of schemes in Fig. 7.

In particular, Fig. 7(a) shows that $\langle S_{d,eq} \rangle$, namely the dynamic effect induced by thunderstorms on structures [53], tends to reduce on increasing both ξ and $\tilde{n}_1$. From a qualitative viewpoint, this trend confirms what has long been known with regard to synoptic winds. From a quantitative viewpoint, instead, the dynamic effects induced by thunderstorms seem to be less sensitive to ξ and $\tilde{n}_1$. The limited dependence of $\langle S_{d,eq} \rangle$ on ξ is typical of the structural response to short duration events, which do not last long enough to trigger full resonance. The interpretation of the limited dependence of $\langle S_{d,eq} \rangle$ on $\tilde{n}_1$ is more delicate [18] and calls for further studies.

9. Application

In spite of a rather complex formulation, the application of the TRST is straightforward. Table 2 provides a synthetic list of its main steps. A calculation example is reported below.

Consider a telecommunication antenna mast [79] made up of two steel shafts with tubular circular cross-section, whose total height is $H = 30$ m (Fig. 8a). The first shaft, referred to as main shaft, is 24 m long; the outer diameter of its cross-section varies from 1100 mm at the bottom to 550 mm at the top; its thickness is constant and equal to 5 mm. The second shaft, put above the first one, is 6 m long; its cross-section has constant outer diameter 193.7 mm and constant thickness 7.1 mm; it carries 6 antennas covered by a fiberglass cylinder with outer diameter 1500 mm. The following steps correspond to the scheme in Table 2.

(1) The structure is placed in the Port of La Spezia. In accordance with some preliminary statistical estimates carried out in [80], the peak wind velocity of thunderstorm outflows at the height $h = 13$ m above ground with return period 50 years is $\hat{v} = 43.8$ m/s; studies are in progress to improve this estimate based on longer acquisitions. The peak gust factor related to a moving average period $T = 30$ s is $\widehat{G} = 1.20$ [59]. Thus, the maximum value of the slowly-varying mean wind velocity at the height h is $\bar{v}_{max} = 43.8/1.20 = 36.5$ m/s (Eq. (8)).

(2) Without any consideration on the best law that represents the vertical profile of the maximum value of the slowly-varying mean wind velocity (Section 2), the model proposed in [64] is adopted herein. Accordingly, the shape function α in Eq. (4) is given by:

$$\alpha(z) = \left(\frac{z}{h}\right)^{1/6} \frac{1 - erf\left(0.70 \cdot \frac{z}{z^*}\right)}{1 - erf\left(0.70 \cdot \frac{h}{z^*}\right)} \tag{70}$$

where *erf* is the error function, $z^* = 6z_m$ is the height above ground for which $\bar{v}_{max}(z^*) = 0.5\bar{v}_m$, z_m is the height for which $\bar{v}_{max} = \bar{v}_m$, $\bar{v}_m$ is the maximum value of $\bar{v}_{max}$ along z. As an example, $z_m = 50$ m and $z^* = 6 \times 50 = 300$ m. Fig. 8(b) shows the vertical profiles of $\bar{v}_{max}$ and $\hat{v}$ (Eqs. (4) and (8)). Since z_m is higher than the height H of the structure, the shape of the wind velocity along the tower is similar to the typical profile of the atmospheric boundary layer.

(3) The density of air is $\rho = 1.25$ kg/m^3. According to the Italian Standards [81], the drag coefficient of the main shaft is $c_D = 0.6$; the drag coefficient of the upper cylinder is $c_D = 0.615$. Fig. 8(c) shows the vertical profile of the peak wind force (Eq. (40)), where $\hat{f}(H) = 1333$ N/m.

(4) The structure is schematized as a slender vertical cantilever beam with elastic linear properties. The first three natural flexural frequencies are $n_1 = 0.92$ Hz, $n_2 = 2.84$ Hz, $n_3 = 7.46$ Hz [79]. The first modal shape is well approximated by the relationship $\psi_1(z) = (z/H)^{\zeta}$, where $\zeta = 2.4$. The

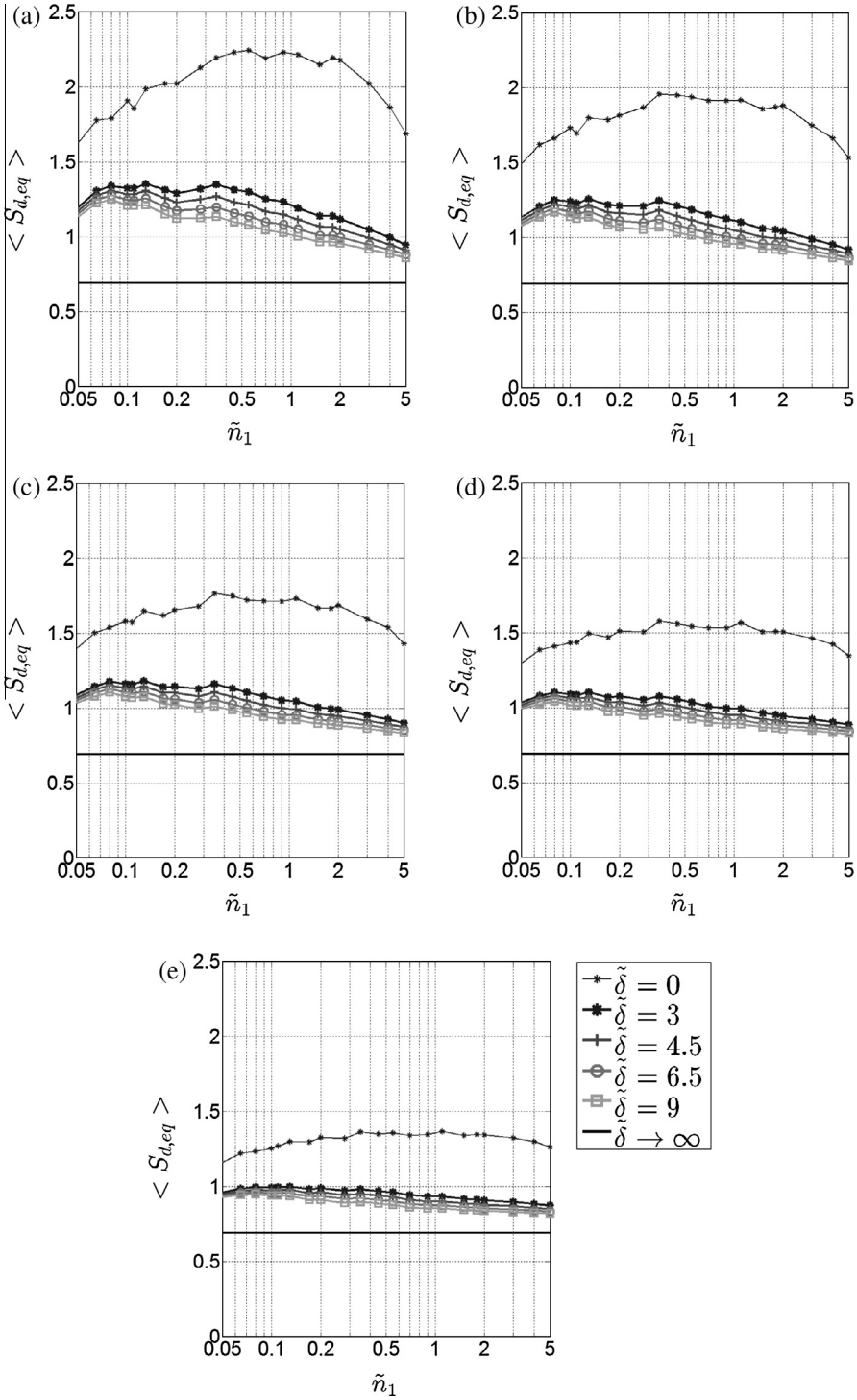

Fig. 5. Mean ERS as a function of $\tilde{n}_1$ and $\tilde{\delta}$ for: (a) $\xi = 0.002$; (b) $\xi = 0.005$; (c) $\xi = 0.01$; (d) $\xi = 0.02$; (e) $\xi = 0.05$.

damping coefficient is $\xi = 0.005$ [82]. The first modal mass is $m_1 = 671$ kg (Eq. (12)). Since the second natural frequency is well beyond the first one, it is reasonable to evaluate the structural response considering only the first mode of vibration.

(5) Thanks to Eq. (20), $a_1 = 6.908$ m^2. The peak static displacement at the top of the structure is $\hat{x}(H) = 0.37$ m (Eq. (41)).

(6) The exponential decay coefficient of the turbulence is assumed as $c_z = 10$ [73], the modal shape factor is $\kappa = 0.5/(2.4 + 1)^{0.55} = 0.255$, the equivalent height is $z_{eq} = 0.6 \times 30 = 18$ m (Eq. (33)), $\alpha(z_{eq}) = 1.041$ (Eq. (70)), $\bar{v}_{max}(z_{eq}) = 36.5 \times 1.041 = 38.0$ m/s (Eq. (4)).

(7) The mean value and the *cov* of the ERS, $S_{d,eq}$, may be evaluated through one of the following methods:

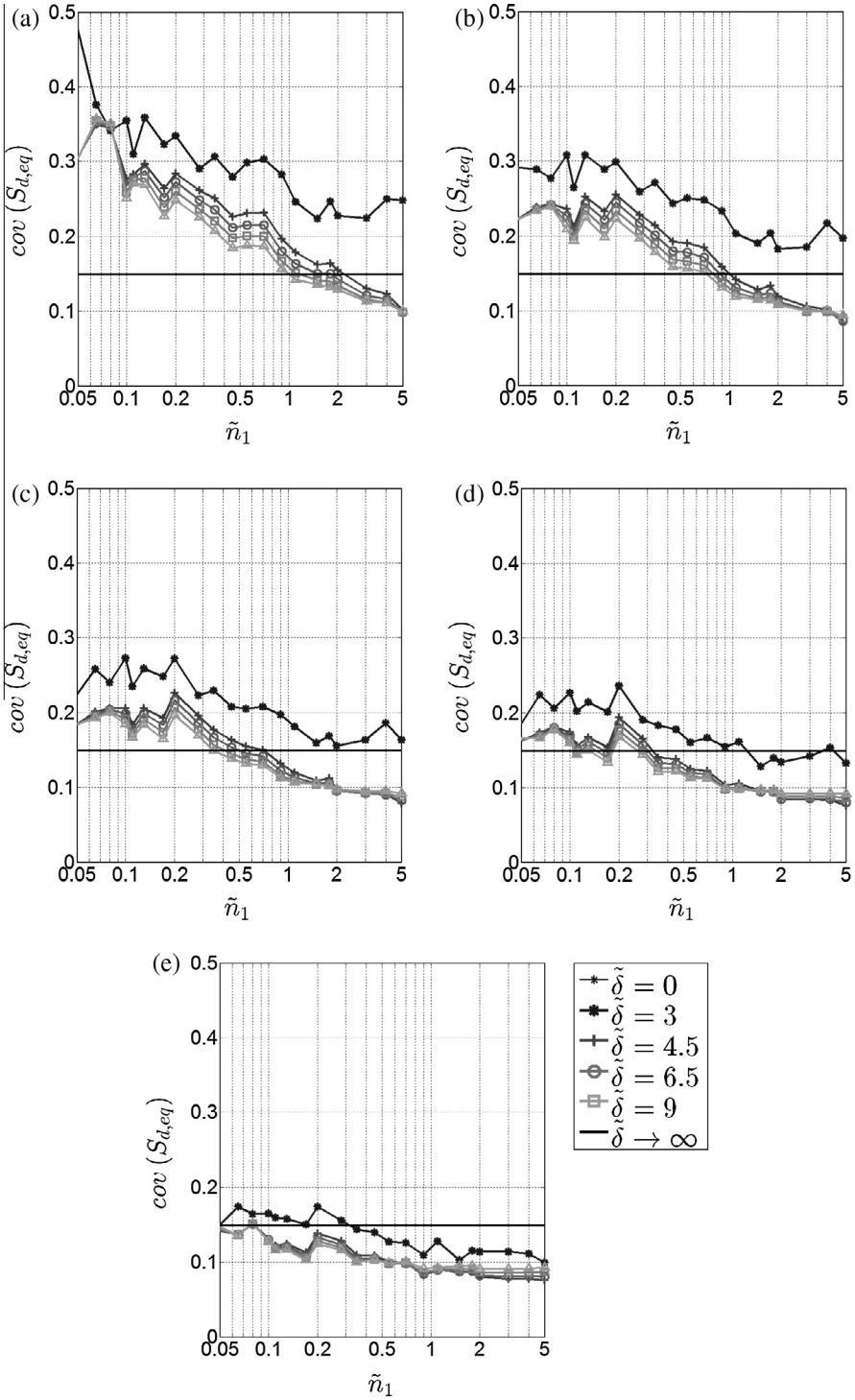

Fig. 6. *Cov* of the ERS as a function of $\tilde{n}_1$ and $\tilde{\delta}$ for: (a) $\xi = 0.002$; (b) $\xi = 0.005$; (c) $\xi = 0.01$; (d) $\xi = 0.02$; (e) $\xi = 0.05$.

(A) In addition to the knowledge of $n_1 = 0.92$ Hz and $\xi = 0.005$, the use of Figs. 3 and 4 calls for evaluating the size factor $\delta = 0.255 \times 10 \times 30/38.0 = 2.01$ m (Eq. (32)). Accordingly, $\langle S_{d,eq} \rangle = 1.20$ and $cov(S_{d,eq}) = 0.14$.

(B) In addition to the knowledge of $\xi = 0.005$, the use of Figs. 5 and 6 calls for evaluating the reduced first natural frequency $\tilde{n}_1 = 0.92 \times 18/38.0 = 0.435$ and the reduced size factor $\tilde{\delta} = 0.255 \times 10/0.6 = 4.25$ (Eqs. (66) and (67)). Accordingly, $\langle S_{d,eq} \rangle = 1.15$ and $cov(S_{d,eq}) = 0.18$.

(C) In addition to the knowledge of $\xi = 0.005$, the use of Fig. 7 calls for evaluating only $\tilde{n}_1 = 0.435$. Accordingly, $\langle S_{d,eq} \rangle = 1.17$ and $cov(S_{d,eq}) = 0.18$.

(8) Table 3 shows, for each of these methods, the mean, the *cov*, the *std* and the mean plus one *std* of the ERS. The *cov* multiplied by 100 corresponds to the per cent increase of the mean plus one *std* with regard to the mean. At least for the structure examined here, the three methods provide very close results; such results become almost invariant with reference to the mean plus one *std* of the ERS.

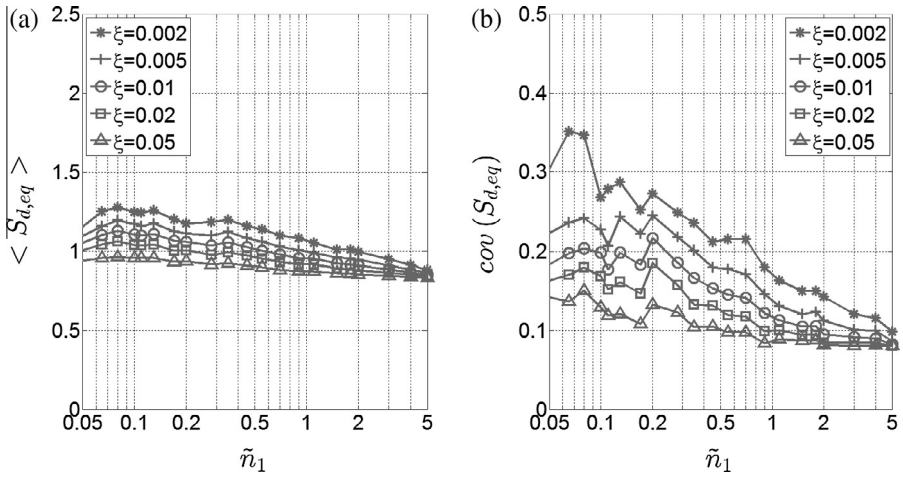

Fig. 7. Mean value (a) and *cov* (b) of the ERS as a function of $\tilde{n}_1$ and ξ, for $\bar{\delta} = 4.5$.

Table 2
Synthesis of the application of the TRST.

Step	Operation
1	Assign the peak wind velocity $\hat{v}$, or the maximum value of the slowly-varying mean wind velocity $\bar{v}_{max}$ at the reference height h; $\hat{v}$ and $\bar{v}_{max}$ are linked by Eq. (8)
2	Select a non-dimensional vertical profile of the wind velocity α (Eq. (4))[a]
3	Assign the height H, the width b, and the drag coefficient c_D of the structure; calculate the peak wind force $\hat{f}$ (Eq. (40))
4	Determine the first natural frequency n_1, the first mode of vibration ψ_1, the damping coefficient ξ, and the first modal mass m_1 (Eq. (12)) of the structure
5	Evaluate the quantity a_1 (Eq. (20)), and the peak static displacement $\hat{x}$ (Eq. (41))
6	Assign the exponential decay coefficient of the turbulence c_z (for instance $c_z = 10$), the modal shape factor κ and the equivalent height z_{eq} (Eq. (33)); evaluate $\bar{v}_{max}$ at the height z_{eq} (Eq. (4))
7	Evaluate the mean value and the *cov* of the ERS $S_{d,eq}$ by one of the following methods: (A) assign the size factor δ (Eq. (32)); estimate $\langle S_{d,eq} \rangle$ (Fig. 3) and $cov(S_{d,eq})$ (Fig. 4) as functions of n_1, ξ, δ (B) assign $\tilde{n}_1$ (Eq. (66)) and $\bar{\delta}$ (Eq. (67)); estimate $\langle S_{d,eq} \rangle$ (Fig. 5) and $cov(S_{d,eq})$ (Fig. 6) as functions of $\tilde{n}_1, \xi, \bar{\delta}$ (C) assign $\tilde{n}_1$ (Eq. (66)); estimate $\langle S_{d,eq} \rangle$ and $cov(S_{d,eq})$ (Fig. 7) as functions of $\tilde{n}_1, \xi$
8	Identify the design ERS by $\langle S_{d,eq} \rangle$ or $\langle S_{d,eq} \rangle + std(S_{d,eq}) = \langle S_{d,eq} \rangle [1 + cov(S_{d,eq})]$ (Eqs. (63)–(65))
9	Evaluate the maximum displacement x_{max} (Eq. (49)) and the equivalent static force f_{eq} (Eq. (50))

[a] In this stage of the research, for sake of simplicity, $\beta = 1$ (Eq. (4)) and $\chi = 1$ (Eq. (8)).

(9) The maximum displacement of the structure and the equivalent static force are furnished by Eqs. (49) and (50), respectively; their application implies an appropriate choice of the design ERS (Section 7, Table 3). Table 4 summarizes the results obtained, at the top of the structure and for the three methods described above, using the mean value of the ERS and its mean value plus one *std*, respectively, as the design ERS. The three methods provide very close results with utmost simplicity. The passage from using the mean ERS to using its mean plus one *std* increases the loading and the response, on average, of about 15%. Moreover, if possible, the results become even more stable.

10. Conclusions and prospects

This paper is part of a research project that lays the foundation of a "new" method aimed at generalizing the "old" RS technique from earthquakes to thunderstorms. A previous paper [53] addressed the problem of point-like SDOF systems subjected to wind actions perfectly coherent over the exposed structural surface. The present paper extends this formulation to real vertical MDOF systems subjected to partially coherent wind fields with assigned velocity profile and turbulence properties. In this stage of the research, for sake of simplicity and without limitations for future developments, the turbulence intensity is independent of the height above ground, the peak velocity profile is proportional to the slowly-varying mean wind velocity profile, the structure is modeled as a continuous slender vertical cantilever beam.

The paper starts from formulating the problem of the dynamic alongwind response of structures to non-stationary thunderstorm outflows, both in the time and frequency domains, considering only the first mode of vibration. Then it adopts the EWST in order to simplify the above formulation and to establish conceptual and operative bases aiming to apply the TRST to MDOF systems. This goal is pursued by introducing the new concept of ERS. It is shown that the RS of a SDOF system subjected to perfectly coherent wind fields depends on the thunderstorm velocity, the fundamental frequency and the damping coefficient; the ERS of a MDOF system subjected to partially correlated wind fields depends on one more parameter, the size factor, that synthesizes the role of the aerodynamic admittance.

It is demonstrated that the ERS admits an upper and a lower bound. The upper bound corresponds to the case in which the wind field is perfectly coherent, or the structural surface exposed to wind is infinitely small, or the aerodynamic admittance is unit; in this situation the ERS for a MDOF system coincides with the RS for a SDOF system. The lower bound corresponds to the case in which the wind field is fully incoherent, or the structural surface exposed to wind is infinitely large, or the aerodynamic admittance is null; in this situation the ERS for a MDOF system coincides with the BRS for a SDOF system.

Two different forms of parameterization are used and discussed: the former expresses the ERS as a function of the first natural frequency and of the size factor; the latter expresses it as a function of two non-dimensional parameters referred to as the reduced first natural frequency and the reduced size factor. Their comparison seems to indicate that the latter is more effective than

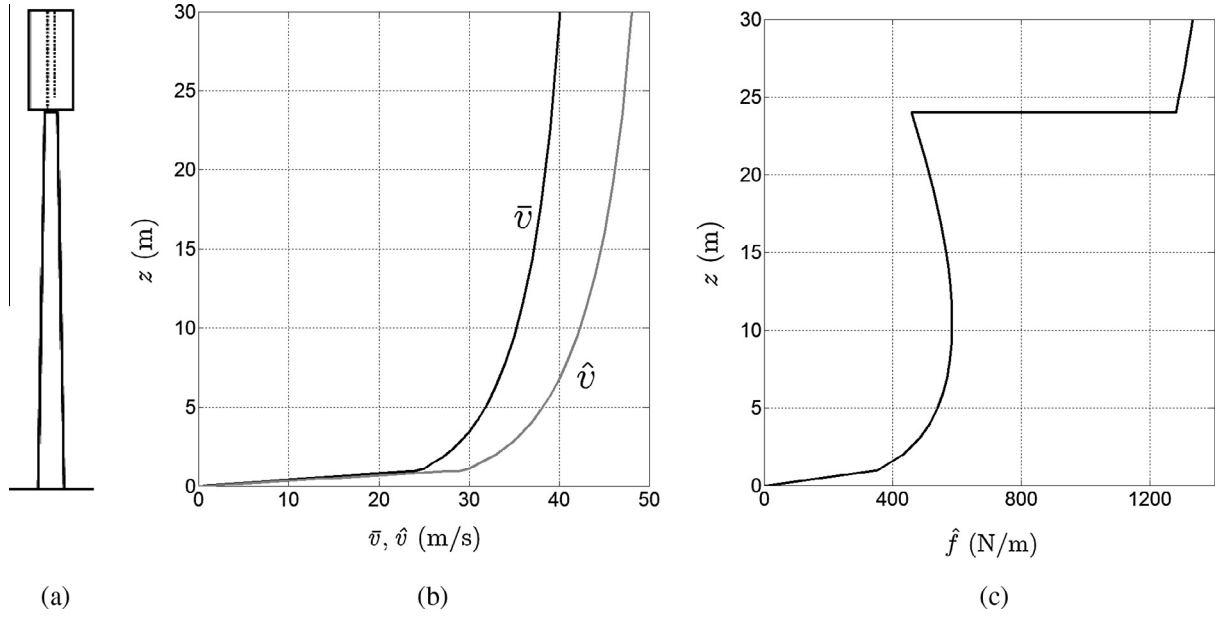

Fig. 8. Telecommunication antenna mast: (a) schematic view; (b) maximum value of the slowly-varying mean wind velocity and peak wind velocity; (c) peak wind force.

Table 3
Mean value, *cov*, *std*, and mean value plus one *std* of the ERS.

Method	$\langle S_{d,eq} \rangle$	$cov(S_{d,eq})$	$std(S_{d,eq})$	$\langle S_{d,eq} \rangle + std(S_{d,eq})$
A	1.20	0.14	0.17	1.37
B	1.15	0.18	0.21	1.36
C	1.17	0.18	0.21	1.38

Table 4
Maximum displacement and equivalent static force at the top of the structure.

Design ERS	$\langle S_{d,eq} \rangle$		$\langle S_{d,eq} \rangle + std(S_{d,eq})$	
Method	$x_{max}(H)$ (m)	$f_{eq}(H)$ (N/m)	$x_{max}(H)$ (m)	$f_{eq}(H)$ (N/m)
A	0.44	1600	0.51	1826
B	0.43	1533	0.50	1812
C	0.43	1560	0.50	1840

the former. It is possible, however, that this remark is influenced by the model adopted to schematize the structure.

Despite a rather complex formulation, the application of the TRST is straightforward. It consists in expressing the equivalent static force as the product of the peak wind force by a non-dimensional quantity, the ERS, provided by a simple diagram. This expression establishes a robust link with the parallel expression of the equivalent static force for synoptic winds. The derivation of the ERS represents one of the most typical features of this method: it involves the joint numerical processing of a set of homogeneous thunderstorm records and the implementation of an analytical model that conceptually reconstructs the complete wind field around the measured data.

The expression of the equivalent static force as provided by the TRST points out four basic ingredients: (1) the design intensity of the ESF, defined through the peak wind velocity or the maximum value of the slowly-varying mean wind velocity at a suitable reference height above ground, with assigned probability of occurrence; (2) the vertical profile of the design wind velocity associated with the thunderstorm outflow; (3) the aerodynamic coefficient of the structure, in prospect including the transient effects due to the limited duration and the rapid variation of the wind actions; (4) the dynamic effects due to aerodynamic admittance and the resonant response of the structure, taken into account through the ERS. This paper defines this analytical and conceptual framework, provides preliminary issues with regard to point (4), confirms the utmost importance of developing future research with reference to points (1), (2) and (3). Despite this remark, in its whole, the great simplicity and the versatility of the TRST make it a profitable tool and a powerful resource for rapid engineering calculations and code provisions.

This paper presents ample room for advances in many directions.

First of all, research is in progress to overcome the simplifying hypotheses according to which the turbulence intensity is independent of height and the peak wind velocity profile is proportional to the slowly-varying mean wind velocity profile. This requests, on the one hand, to generalize the TRST framework in order to accommodate more flexible definitions of these quantities, on the other hand, to carry out further research aiming to improve the knowledge of the thunderstorm outflows; this relies on recent advances in field monitoring, wind tunnel tests and CFD simulations.

Evaluations are being carried out with reference to the many thunderstorm records already detected by the monitoring network of the projects “Wind and Ports” and “Wind, Ports, and Sea” and not yet examined [59], including the vertical velocity profiles recorded by LiDARs. Enriching the catalogue of the thunderstorm records is a key step, on the one hand, to improve the knowledge of the RS, on the other hand, to deal with the crucial issue of the statistical evaluation of the design wind velocity of thunderstorm outflows. In parallel, it is greatly advised that other groups that avail of similar measurements may apply the TRST in order to inspect the different features involved by thunderstorms in different parts of the world and their consequences on structures. The Genoese wind engineering group is opened to carry out joint comparisons and analyses.

Studies are also in progress to generalize the procedure limited here to slender vertical structures to a wider class of building types. There is the aim of inspecting the role of the higher modes of vibration, focusing attention on their importance with regard to the quasi-static and the resonant parts of the response, likewise the consequences of the sudden changes of direction that frequently occur in the course of thunderstorm. Though the extension of the EWST from stationary to non-stationary phenomena has already been the subject of several studies with largely favorable outcome, the development of a systematic validation of this method and the TRST is in progress, based on a new strategy for

the Monte Carlo simulation of thunderstorm outflows. Research will be developed to generalize the TRST to different types of non-stationary wind phenomena.

Finally, a comparative study between the dynamic response of structures to extra-tropical cyclones and thunderstorms remains to be conducted in order to clarify, for different construction types and environmental conditions, the main qualitative and quantitative prerogatives of these two phenomena.

Acknowledgements

The data exploited for this research has been recorded by the wind monitoring network of the projects "Winds and Ports" and "Wind, Ports and Sea", financed by European Territorial Cooperation Objective, Cross-border program Italy–France Maritime 2007–2013. Author thankfully acknowledges the cooperation of the Port Authorities of Genoa, La Spezia, Livorno, Savona and Bastia.

Appendix A. List of main symbols, operators and acronyms

List of symbols

$a_1, \tilde{a}'_1$	quantities defined by Eqs. (20) and (21)
A_1, A'_1	quantities defined by Eqs. (24) and (27)
b	width of the structural surface exposed to wind
c_D	drag coefficient
c_z	exponential decay coefficient of $\tilde{v}'$ along z
$Coh_{\tilde{v}'\tilde{v}'}$	coherence function of $\tilde{v}'$ (Eqs. (6) and (29))
d, d_{max}	reduced displacement (Eq. (54)) and its maximum value for a SDOF system
$\bar{d}, \bar{d}_{max}$	reduced mean displacement (Eq. (59)) and its maximum value for a SDOF system
$d_{eq}, d_{eq,max}$	reduced equivalent displacement (Eq. (47)) and its maximum value for a MDOF system
$f, \bar{f}, f', \hat{f}, f_{eq}$	force (Eqs. (9) and (14)), slowly-varying mean part (Eq. (15)) and residual fluctuating part (Eqs. (16) and (35)) of f, peak force (Eq. (40)), and equivalent static force (Eq. (50))
$f_1, \bar{f}_1, f'_1$	first modal force (Eqs. (13) and (17)), slowly-varying mean part (Eq. (18)) and residual fluctuating part (Eqs. (19) and (36)) of f_1
$\widehat{G}$	peak gust factor defined by Eq. (8)
h, H	reference height above ground and height of the structure
h_1, H_1	impulse response function (Eq. (25)) and complex frequency response function (Eq. (B.3)) of the first principal coordinate
i	imaginary unit
$I_v, \bar{I}_v$	slowly-varying turbulence intensity (Eq. (5)) and its average value
m, m_1	mass per unit length and first modal mass (Eq. (12))
n, n_0, n_1	frequency, fundamental frequency of a SDOF system, and first natural frequency
$\tilde{n}, \tilde{n}_1$	reduced frequency and reduced first natural frequency (Eq. (66))
$p_1, \bar{p}_1, p'_1$	first principal coordinate (Eq. (22)), slowly-varying mean part (Eq. (23)) and residual fluctuating part of p_1
$S_{\tilde{v}'\tilde{v}'}, S_{\tilde{v}'}, S_{\tilde{v}',eq}$	CPSD (Eq. (6)) and PSD of $\tilde{v}'$, PSD of $\tilde{v}'_{eq}$ (Eq. (30))
$S_{\tilde{a}'_1}, S_{p'_1}$	PSD of $\tilde{a}'_1$ (Eqs. (28) and (39)) and p'_1 (Eqs. (26) and (37))
$S_d, S_{db}, S_{d,eq}$	RS (Eq. (55)) and BRS (Eq. (60)) of a SDOF system, ERS (Eq. (48)) of a MDOF system
$t, \tilde{t}$	time and reduced time
T	moving average period
$u, \bar{u}, u_{eq}$	reduced wind velocity (Eq. (53)), reduced slowly-varying mean wind velocity (Eq. (58)), and reduced equivalent wind velocity (Eq. (42))
$v, \bar{v}, v', v_{eq}$	wind velocity (Eqs. (1), (3) and (7)), slowly-varying mean wind velocity (Eq. (4)), residual fluctuating wind velocity (Eq. (2)), and equivalent wind velocity (Eq. (34))
$\bar{v}_{max}, \hat{v}$	maximum value of $\bar{v}$ (Eq. (4)) and peak wind velocity (Eq. (8));
$\tilde{v}', \tilde{v}'_{eq}$	reduced turbulent fluctuation (Eq. (2)) and reduced equivalent turbulent fluctuation
$\widetilde{V}', \widetilde{V}'_{eq}$	Fourier transforms of $\tilde{v}'$ and $\tilde{v}'_{eq}$
$x, \hat{x}, x_{max}$	displacement (Eq. (10)), peak static displacement (Eq. (41)), and maximum displacement (Eq. (49))
z, z'	heights above ground
z_{eq}	equivalent height (Eq. (33))
α, β, χ	non-dimensional functions of z that define the shape of the vertical profiles of $\bar{v}$ (Eq. (4)), I_v (Eq5) and $\hat{v}$ (Eq. (8))
$\delta, \tilde{\delta}$	size factor (Eq. (32)) and reduced size factor (Eq. (67));
γ, γ_{max}	non-dimensional function of t that expresses the time variation of $\bar{v}$ (Eq. (4)) and its maximum value
κ	modal shape factor (Eq. (33))
$\mu, \bar{\mu}$	non-dimensional function of t that expresses the time variation of I_v (Eq. (5)) and its average value
ρ	density of air
σ_v	slowly-varying standard deviation of the residual velocity fluctuation v' (Eq. (2))
τ	short time interval over which the peak wind velocity $\hat{v}$ is averaged
ξ	damping coefficient
ψ_1	first modal shape
ζ	exponent of the power law that approximates ψ_1
ΔT	time interval between 10 min and 1 h

List of operators

C	operator defined by Eq. (31)
erf	error function
F, F^{-1}	Fourier transform and inverse Fourier transform
$\langle\,\rangle$, *std*, *cov*	mean value, standard deviation and coefficient of variation

List of acronyms

EWST	Equivalent Wind Spectrum Technique
PSD, CPSD	Power Spectral Density and Cross-Power Spectral Density
RS, BRS, ERS	Response Spectrum and Base Response Spectrum for SDOF systems, Equivalent Response Spectrum for MDOF systems
SDOF, MDOF	Single- and Multi-Degree-Of-Freedom
TRST	Thunderstorm Response Spectrum Technique

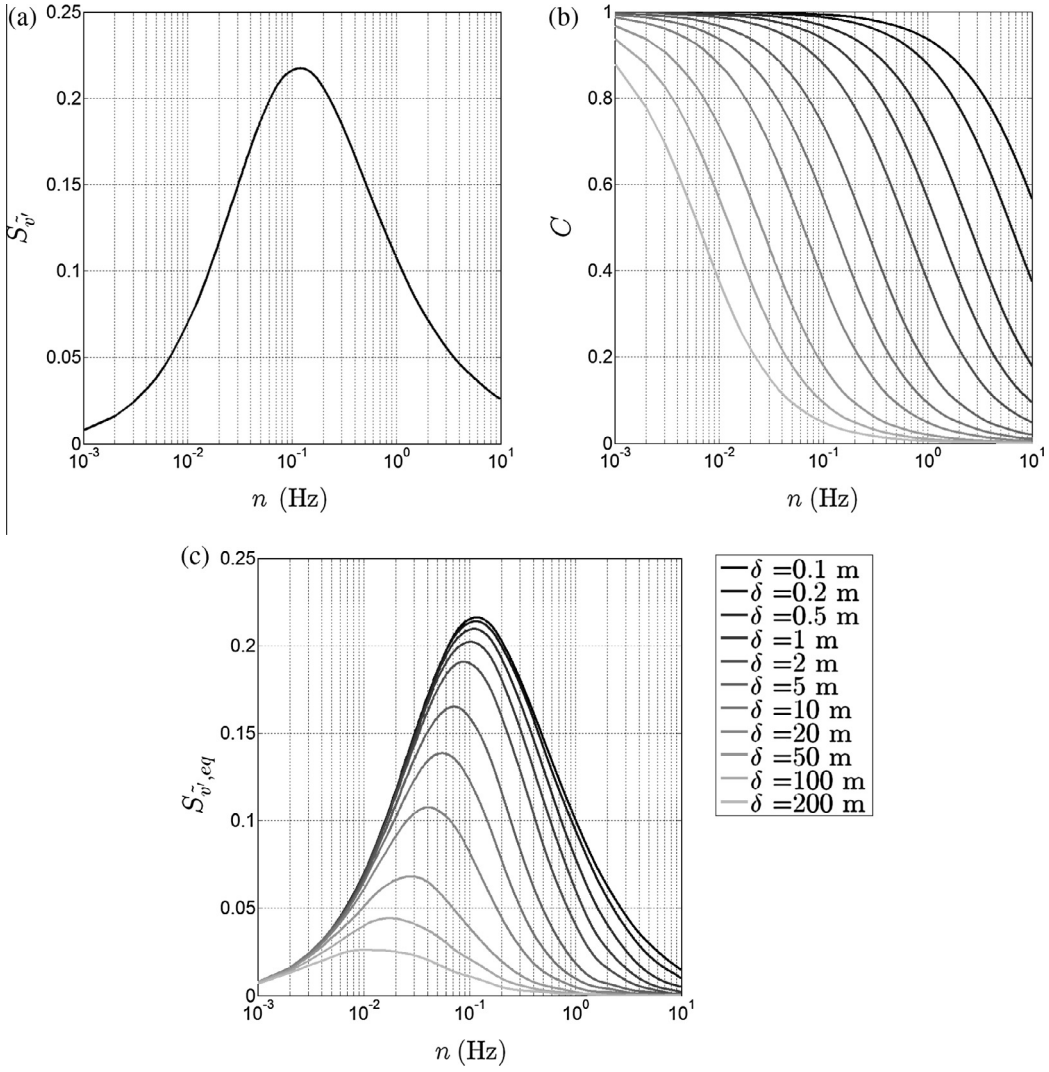

Fig. C.1. (a) Typical PSD of $\tilde{v}'$; (b) C as a function of δ; (c) PSD of $\tilde{v}'_{eq}$ as a function of δ.

Appendix B. Quasi-static response

Section 3 provides a general outline of the dynamic response of structures to non-stationary wind fields. Observing that the duration of thunderstorms is usually much greater than the first natural period of structures [59], $T_1 = 1/n_1$, and assuming that the time t at which $\gamma = \gamma_{max} = 1$ (Eq. (4)) is sufficiently large, Eqs. (24) and (27) may be approximated by the relationships [45]:

$$A_1(t) = \frac{\gamma^2(t)}{m_1(2\pi n_1)^2} \tag{B.1}$$

$$A'_1(n,t) = \gamma^2(\tau)\mu(\tau)H_1(n) \tag{B.2}$$

where H_1 is the complex frequency response function of p_1, namely the Fourier transform of h_1 (Eq. (25)):

$$H_1(n) = \frac{1}{m_1(2\pi n_1)^2}\frac{1}{1-\frac{n^2}{n_1^2}+2i\xi\frac{n}{n_1}} \tag{B.3}$$

In other words, excluding unrealistically low values of n_1, the structure responds quasi-statically to the transient thunderstorm loading. This result is confirmed by embedding the data reported by [59] into the gust front factor framework provided in [43].

Appendix C. Reduced equivalent turbulent fluctuation

This appendix depicts the application of the EWST through an example referred to the structure studied in Section 9. Fig. C.1(a) shows the PSD of the reduced turbulent fluctuation $\tilde{v}'$, based on the tentative model proposed for thunderstorm outflows in [59], in correspondence of $z = z_{eq} = 18$ m and $\bar{v}_{max}(z_{eq}) = 38.0$ m/s (Section 9). Fig. C.1(b) shows the diagrams of Eq. (31) for a typical set of size factors $\delta = 0.1$–200 m. Fig. C.1(c) shows the PSD of the reduced equivalent turbulent fluctuation $\tilde{v}'_{eq}$ (Eq. (30)), pointing out the filtering effect of C. On increasing δ, similarly to the aerodynamic admittance, C progressively elides the high frequency harmonic content of $\tilde{v}'$.

Appendix D. Spectral analysis of the reduced equivalent turbulence

Let us consider the reduced turbulent fluctuation $\tilde{v}'$ at the eight h above ground. Accordingly, let as define the following function [78]:

$$\tilde{v}'_{\Delta T}(h,t) = \tilde{v}'(h,t) \quad \text{for} \quad t \in (-\Delta T/2, \Delta T/2) \tag{D.1a}$$

$$\tilde{v}'_{\Delta T}(h,t) = 0 \quad \text{elsewhere} \tag{D.1b}$$

Assuming that $\tilde{v}'$ is a sample function of an ergodic process, the PSD of $\tilde{v}'$ is given by:

$$S_{\tilde{v}'}(h,n) = \lim_{\Delta T\to\infty} \frac{|\widetilde{V}'_{\Delta T}(h,n)|^2}{2\pi\Delta T} \tag{D.2}$$

where $\widetilde{V}'_{\Delta T}$ is the Fourier transform of $\tilde{v}'_{\Delta T}$. Analogously, the PSD of the reduced equivalent turbulent fluctuation $\tilde{v}'_{eq}$ is given by:

$$S_{\tilde{v}',eq}(n,\delta) = \lim_{\Delta T\to\infty} \frac{|\widetilde{V}'_{\Delta T,eq}(n,\delta)|^2}{2\pi\Delta T} \tag{D.3}$$

where $\widetilde{V}'_{\Delta T,eq}$ is the Fourier transform of the function $\tilde{v}'_{\Delta T,eq}$ defined as:

$$\tilde{v}'_{\Delta T,eq}(t,\delta) = \tilde{v}'_{eq}(t,\delta) \quad \text{for} \quad t\in(-\Delta T/2,\Delta T/2) \tag{D.4a}$$

$$\tilde{v}'_{\Delta T,eq}(t,\delta) = 0 \quad \text{elsewhere} \tag{D.4b}$$

Assuming that ΔT is sufficiently long, Eqs. (D.2) and (D.3) may be approximated as:

$$S_{\tilde{v}'}(h,n) = \frac{|\widetilde{V}'(h,n)|^2}{2\pi\Delta T} \tag{D.5}$$

$$S_{\tilde{v}',eq}(n,\delta) = \frac{|\widetilde{V}'_{eq}(n,\delta)|^2}{2\pi\Delta T} \tag{D.6}$$

Let us assume, as in Section 6, that $S_{\tilde{v}'}(z_{eq},n) = S_{\tilde{v}'}(h,n)$. Replacing Eqs. (D.5) and (D.6) into Eq. (30), this may be rewritten as:

$$|\widetilde{V}'_{eq}(n,\delta)|^2 = |\widetilde{V}'(h,n)|^2 C(\delta n) \tag{D.7}$$

Eq. (62) derives from Eq. (D.7), remembering that C is a real positive function (Eq. (31)).

Appendix E. Equivalent response spectrum generalized assessment

In the framework of the parameterization described in Section 8, the assessment procedure of the ERS illustrated in Section 7 may be generalized as follows:

(1) Consider $v(h,t)$ and extract $\tilde{v}'(h,\tilde{t})$ and $\hat{v}(h)$ (Eq. (7)).
(2) Evaluate $\widetilde{V}'(h,\tilde{n}) = F\{\tilde{v}'(h,\tilde{t})\}$.
(3) Evaluate $\widetilde{V}'_{eq}(\tilde{n},\tilde{\delta}) = \widetilde{V}'(h,\tilde{n})\sqrt{C(\tilde{\delta}\tilde{n})}$ (Eq. (62)), being $\tilde{\delta} = \tilde{\delta}_j (j = 1,2,\ldots,\widetilde{J})$ (Eq. (67)).
(4) Evaluate $\tilde{v}'_{eq}(\tilde{t},\tilde{\delta}) = F^{-1}\{\widetilde{V}'_{eq}(\tilde{n},\tilde{\delta})\}, \tilde{\delta} = \tilde{\delta}_j (j = 1,2,\ldots,\widetilde{J})$.
(5) Replace $\tilde{v}'_{eq}(\tilde{t},\tilde{\delta})$ into Eq. (34), and determine $v_{eq}(h,\tilde{t},\tilde{\delta}), \tilde{\delta} = \tilde{\delta}_j (j = 1,2,\ldots,\widetilde{J})$.
(6) Replace $v_{eq}(h,\tilde{t},\tilde{\delta})$ into Eq. (42), and determine $u_{eq}(\tilde{t},\tilde{\delta}), \tilde{\delta} = \tilde{\delta}_j (j = 1,2,\ldots,\widetilde{J})$.
(7) Replace $u_{eq}(\tilde{t},\tilde{\delta})$ into Eq. (47), and determine $d_{eq}(\tilde{t}), \tilde{\delta} = \tilde{\delta}_j (j = 1,2,\ldots,\widetilde{J}), \tilde{n}_1 = \tilde{n}_{1l} (l = 1,2,\ldots,\widetilde{L}), \xi = \xi_m (m = 1,2,\ldots,M)$.
(8) Determine $S_{d,eq}$ (Eq. (48)), $\tilde{\delta} = \tilde{\delta}_j (j = 1,2,\ldots,\widetilde{J}), \tilde{n}_1 = \tilde{n}_{1l} (l = 1,2,\ldots,\widetilde{L}), \xi = \xi_m (m = 1,2,\ldots,M)$.

Repeating the above procedure for a set of N homogeneous thunderstorm records, the mean value, the *std* and the *cov* of $S_{d,eq}$ are provided by Eqs. (63)–(65).

References

[1] Bjerknes J, Solberg H. Life cycle of cyclones and the polar front theory of atmospheric circulation. Geophys Publ 1922;3:3–18.
[2] Davenport AG. The application of statistical concepts to the wind loading of structures. Proc Inst Civ Eng 1961;19:449–72.
[3] Davenport AG. Note on the distribution of the largest value of a random function with application to gust loading. Proc Inst Civ Eng 1964;24:187–96.
[4] Davenport AG. Gust loading factors. J Struct Div ASCE 1967;93(ST3):11–34.
[5] Solari G. Alongwind response estimation: closed form solution. J Struct Div ASCE 1982;108(1):225–44.
[6] Solari G. Analytical estimation of the alongwind response of structures. J Wind Eng Ind Aerodyn 1983;14:467–77.
[7] Solari G. Gust buffeting. II: dynamic alongwind response. J Struct Eng ASCE 1993;119(2):383–98.
[8] Solari G, Kareem A. On the formulation of ASCE7-95 gust effect factor. J Wind Eng Ind Aerodyn 1998;77&78:673–84.
[9] Piccardo G, Solari G. Closed form prediction of 3-D wind-excited response of slender structures. J Wind Eng Ind Aerodyn 1998;74–76:697–708.
[10] Piccardo G, Solari G. 3-D gust effect factor for slender vertical structures. Prob Eng Mech 2002;17:143–55.
[11] Zhou Y, Kareem A. Gust loading factor: new model. J Struct Eng ASCE 2001;127:168–75.
[12] Holmes JD. Effective static load distributions in wind engineering. J Wind Eng Ind Aerodyn 2002;90:91–109.
[13] Repetto MP, Solari G. Equivalent static wind actions on vertical structures. J Wind Eng Ind Aerodyn 2004;92:335–57.
[14] Byers HR, Braham RR. The thunderstorm: final report of the Thunderstorm Project. Washington: U.S. Government Printing Office; 1949.
[15] Fujita TT. Downburst: microburst and macroburst. Chicago: University of Chicago Press; 1985.
[16] Fujita TT. Downburst: meteorological features and wind field characteristics. J Wind Eng Ind Aerodyn 1990;36:75–86.
[17] Letchford CW, Mans C, Chay MT. Thunderstorms – their importance in wind engineering (a case for the next generation wind tunnel). J Wind Eng Ind Aerodyn 2002;90:1415–33.
[18] Solari G. Emerging issues and new scenarios for wind loading on structures in mixed climates. Wind Struct 2014;19(3):295–320.
[19] Mason MS, Letchford CW, James DL. Pulsed wall jet simulation of a stationary thunderstorm downburst. Part A: physical structure and flow field characterization. J Wind Eng Ind Aerodyn 2005;93:557–80.
[20] Sengupta A, Sarkar PP. Experimental measurement and numerical simulation of an impinging jet with application to thunderstorm microburst winds. J Wind Eng Ind Aerodyn 2008;96:345–65.
[21] Zhang Y, Sarkar P, Hu H. An experimental study of flow fields and wind loads on gable-roof building models in microburst-like wind. Exp Fluids 2013;54(1511):1–23.
[22] Hangan H. The Wind Engineering Energy and Environment (WindEEE) Dome at Western University, Canada. J Wind Eng JAWE 2014;39:350–1.
[23] Mason M, Fletcher DF, Wood GS. Numerical simulation of idealised three-dimensional downburst wind fields. Eng Struct 2010;32:3558–70.
[24] Vermeire BC, Orf LG, Savory E. Improved modeling of downburst outflows for wind engineering applications using a cooling source approach. J Wind Eng Ind Aerodyn 2011;99:801–14.
[25] Zhang Y, Hu H, Sarkar PP. Modeling of microburst outflows using impinging jet and cooling source approaches and their comparison. Eng Struct 2013;56:779–93.
[26] Aboshosha H, Bitsuamlak G, El Damatty A. Turbulence characterization of downbursts using LES. J Wind Eng Ind Aerodyn 2015;136:44–61.
[27] Ponte Jr J, Riera JD. Wind velocity field during thunderstorms. Wind Struct 2007;10(3):287–300.
[28] Li C, Li QS, Xiao YQ, Ou JP. A revised empirical model and CFD simulations for 3D axisymmetric steady-state flows of downbursts and impinging jets. J Wind Eng Ind Aerodyn 2012;102:48–60.
[29] Abd-Elaal E, Mills JE, Ma X. An analytical model for simulating steady state flows of downburst. J Wind Eng Ind Aerodyn 2013;115:53–64.
[30] Abd-Elaal E, Mills JE, Ma X. Empirical models for predicting unsteady-state downburst wind speeds. J Wind Eng Ind Aerodyn 2014;129:49–63.
[31] Savory E, Parke GAR, Zeinoddini M, Toy N, Disney P. Modelling of tornado and microburst-induced wind loading and failure of a lattice transmission tower. Eng Struct 2001;23:365–75.
[32] Darwish MD, El Damatty AA. Behavior of self-supported transmission line towers under stationary downburst loading. Wind Struct 2011;14(5):481–98.
[33] Aboshosha H, El Damatty A. Engineering method for estimating the reactions of transmission line conductors under downburst winds. Eng Struct 2015;99:272–84.
[34] Ponte Jr J, Riera JD. Simulation of extreme wind series caused by thunderstorms in temperate latitudes. Struct Saf 2010;32(4):131–7.
[35] Xu Z, Hangan H. Scale, boundary and inlet condition effects on impinging jets. J Wind Eng Ind Aerodyn 2008;96:2383–402.
[36] Choi ECC, Hidayat FA. Dynamic response of structures to thunderstorm winds. Prog Struct Eng Mater 2002;4:408–16.
[37] Chen L, Letchford CW. A deterministic-stochastic hybrid model of downbursts and its impact on a cantilevered structure. Eng Struct 2004;26(5):619–29.
[38] Chen L, Letchford CW. Numerical simulation of extreme winds from thunderstorm downbursts. J Wind Eng Ind Aerodyn 2007;95:977–90.
[39] Holmes JD, Hangan HM, Schroeder JL, Letchford CW, Orwig KD. A forensic study of the Lubbock-Reese downdraft of 2002. Wind Struct 2008;11(2):19–39.

[40] Chen L, Letchford CW. Parametric study on the alongwind response of the CAARC building to downbursts in the time domain. J Wind Eng Ind Aerodyn 2004;92(9):703–24.
[41] Chay M, Albermani F. Dynamic response of a SDOF system subjected to simulated downburst winds. In: Proceedings of the 6th Asia–Pacific conference on wind engineering, Seoul, Korea; 2005.
[42] Holmes J, Forristall G, McConochie J. Dynamic response of structures to thunderstorm winds. In: Proceedings of the 10th Americas conference on wind engineering, Baton Rouge, LA; 2005.
[43] Kwon DK, Kareem A. Gust-front factor: new framework for wind load effects on structures. J Struct Eng ASCE 2009;135(6):717–32.
[44] Kwon DK, Kareem A. Generalized gust-front factor: a computational framework for wind load effects. Eng Struct 2013;48:635–44.
[45] Chen X. Analysis of alongwind tall building response to transient nonstationary winds. J Struct Eng ASCE 2008;134(5):782–91.
[46] Huang G, Chen X, Liao H, Li M. Predicting of tall building response to non-stationary winds using multiple wind speed samples. Wind Struct 2013;17 (2):227–44.
[47] Le TH, Caracoglia L. Reduced-order wavelet-Galerkin solution for the coupled, nonlinear stochastic response of slender buildings in transient winds. J Sound Vib 2015;344:179–208.
[48] Tamura Y, Kareem A, Solari G, Kwok KCS, Holmes JD, Melbourne WH. Aspects of the dynamic wind-induced response of structures and codification. Wind Struct 2005;8(4):251–68.
[49] Gomes L, Vickery BJ. Extreme wind speeds in mixed climates. J Wind Eng Ind Aerodyn 1977/1978;2:331–44.
[50] Kasperski M. A new wind zone map of Germany. J Wind Eng Ind Aerodyn 2002;90:1271–87.
[51] Housner GW. Behavior of structures during earthquakes. J Mech Div ASCE 1959;85(EM4):109–29.
[52] Housner GW, Martel RR, Alford JL. Spectrum analysis of strong-motion earthquakes. Bull Seismol Soc Am 1953;43(2):97–119.
[53] Solari G, De Gaetano P, Repetto MP. Thunderstorm response spectrum: fundamentals and case study. J Wind Eng Ind Aerodyn 2015;143:62–77.
[54] Solari G. Wind response spectrum. J Eng Mech ASCE 1989;115(9):2057–73.
[55] Solari G. Equivalent wind spectrum technique: theory and applications. J Struct Eng ASCE 1988;114(6):1303–23.
[56] Piccardo G, Solari G. Generalized equivalent spectrum technique. Wind Struct 1998;1(2):161–74.
[57] Solari G, Repetto MP, Burlando M, De Gaetano P, Pizzo M, Tizzi M, Parodi M. The wind forecast for safety and management of port areas. J Wind Eng Ind Aerodyn 2012;104–106:266–77.
[58] De Gaetano P, Repetto MP, Repetto T, Solari G. Separation and classification of extreme wind events from anemometric records. J Wind Eng Ind Aerodyn 2014;126:132–43.
[59] Solari G, Burlando M, De Gaetano P, Repetto MP. Characteristics of thunderstorms relevant to the wind loading of structures. Wind Struct 2015;20(6):763–91.
[60] McCullough M, Kwon DK, Kareem A, Wang L. Efficacy of averaging interval for nonstationary winds. J Eng Mech ASCE 2014;140(1):1–19.
[61] Oseguera RM, Bowles RL. A simple analytic 3-dimensional downburst model based on boundary layer stagnation flow. NASA Technical Memorandum 100632; 1988.
[62] Vicroy DD. A simple, analytical, axisymmetric microburst model for downdraft estimation. NASA Technical Memorandum No. 104053; 1991.
[63] Vicroy DD. Assessment of micro burst models for downdraft estimation. J Aircraft 1992;29(6):1043–8.
[64] Wood GS, Kwok KCS. An empirically derived estimate for the mean velocity profile of a thunderstorm downburst. In: Proceedings of the 7th Australian wind engineering society workshop, Auckland, Australia; 1998.
[65] Xu Z, Hangan H, Yu P. Analytical solutions for a family of Gaussian impinging jets. J Appl Mech 2008;75(2):021019 (1–12).
[66] Holmes JD, Oliver SE. An empirical model of a downburst. Eng Struct 2000;22 (9):1167–72.
[67] Chay MT, Albermani F, Wilson B. Numerical and analytical simulation of downburst wind loads. Eng Struct 2006;28(2):240–54.
[68] Duranona V, Sterling M, Baker CJ. An analysis of extreme non-synoptic winds. J Wind Eng Ind Aerodyn 2006;95:1007–27.
[69] Orwig KD, Schroeder JL. Near-surface wind characteristics of extreme thunderstorm outflows. J Wind Eng Ind Aerodyn 2007;95:565–84.
[70] Lombardo FT, Smith DA, Schroeder JL, Mehta KC. Thunderstorm characteristics of importance to wind engineering. J Wind Eng Ind Aerodyn 2014;125:121–32.
[71] Gunter WS, Schroeder JL. High-resolution full-scale measurements of thunderstorm outflow winds. J Wind Eng Ind Aerodyn 2015;138:13–26.
[72] Burlando M, De Gaetano P, Pizzo M, Repetto MP, Solari G, Tizzi M. The European project "Wind, Ports and Sea". In: Proceedings of the 14th international conference on wind engineering, Porto Alegre, Brazil; 2015.
[73] Solari G, Piccardo G. Probabilistic 3-D turbulence modeling for gust buffeting of structures. Prob Eng Mech 2001;16(1):73–86.
[74] Solari G, Tubino F. A turbulence model based on principal components. Prob Eng Mech 2002;17:327–35.
[75] Priestley MB. Evolutionary spectra and non-stationary processes. J R Stat Soc B 1965;27(2):204–37.
[76] Lin YK, Cai GQ. Probabilistic structural dynamics. New York: McGraw-Hill; 2004.
[77] Lutes LD, Sarkani S. Random vibration: analysis of structural and mechanical systems. New York: Elsevier; 2004.
[78] Priestley MB. Spectral analysis and time series. London: Academic Press; 1981.
[79] Repetto MP, Solari G. Wind-induced fatigue collapse of real slender structures. Eng Struct 2010;32:3888–98.
[80] Solari G, De Gaetano P, Repetto MP. Wind loading and response of structures in mixed climates. In: Proceedings of the 8th Asia–Pacific conference on wind engineering, Chennai, India; 2013.
[81] CNR-DT 207/2008. Instructions for assessing wind actions and effects on structures. Rome, Italy; 2009.
[82] Pagnini LC, Solari G. Damping measurements of steel poles and tubular structures. Eng Struct 2001;23:1085–95.